

# Syntheses, Characterization and Modification of Transition Metal Octacarboxyphenoxy Phthalocyanines Complex on Gold Electrode

Akinyemi, A.A. (Phd)<sup>1</sup>; Mashazi, P.N. (Phd)<sup>2</sup>

<sup>1</sup>Chemistry Department Education, Lagos State University of Education, Ijanikin Campus, Lagos State, Nigeria.

<sup>2</sup>Rhodes University, Eastern Cape, Grahamstown, South Africa.

Publication Date: 2025/03/29

**Abstract:** The materials used in this work were the first-row transition metals octacarboxyphenoxy phthalocyanines complexes. The complexes were synthesized and immobilized onto gold electrode surfaces. The immobilization method used to modify gold electrode was highly stable. The complexes improved the efficiency of the gold electrodes. Modification of electrodes with MPcs protects the electrode surfaces from chemical fouling, provides enhanced catalytic properties, improves sensitivity and selectivity. The complex and the electrode surfaces were characterized using Fourier transforms infrared (FT-IR) spectroscopy, Ultra-violet Spectroscopy, Mass spectroscopy (MS), Magnetic circular dichroism (MCD), Nuclear magnetic resonance spectroscopy (NMR), Ultraviolet/visible absorption spectroscopy (UV-Vis), Elemental Analysis

**Keywords:** Octacarboxyphenoxy Phthalocyanines, First-Row Transition Metals, Gold Electrode, Immobilization Method.

**How to Cite:** Akinyemi, A.A. (Phd); Mashazi, P.N. (Phd) (2025). Syntheses, Characterization and Modification of Transition Metal Octacarboxyphenoxy Phthalocyanines Complex on Gold Electrode. International Journal of Innovative Science and Research Technology, 10(3), 2472-2491. <https://doi.org/10.38124/ijisrt/25feb1230>

## I. INTRODUCTION

Metallophthalocyanines (MPc) are blue-green anisotropic complexes with planar structure. MPc is aromatic compounds, highly conjugated with 18  $\pi$ -electrons in the macrocyclic ring [1]. The metal ion centre can contain transition metals known for its excellent electroactive properties. The transition metals have varied oxidation states and therefore improve the electrocatalytic activity of MPc-based electrochemical sensors [2]. The complex, MPc consists of four isoindole units fused at their 1,3-positions by nitrogen atoms of aza-bridges. They have a similar core structure of the naturally occurring metalloporphyrin complexes (MPP) but have an extended conjugation of benzene rings. The substituents attached to the ring and the sequestered metal ion at the core centre influence the intrinsic properties and increase the variety of metallophthalocyanines. The terminal ends of MPc can be substituted with functional groups like alkyl, aryl, amino, carboxyl, hydroxyl, thiol and azide [3]. Figure 1 shows the structure of a typical MPc complex.

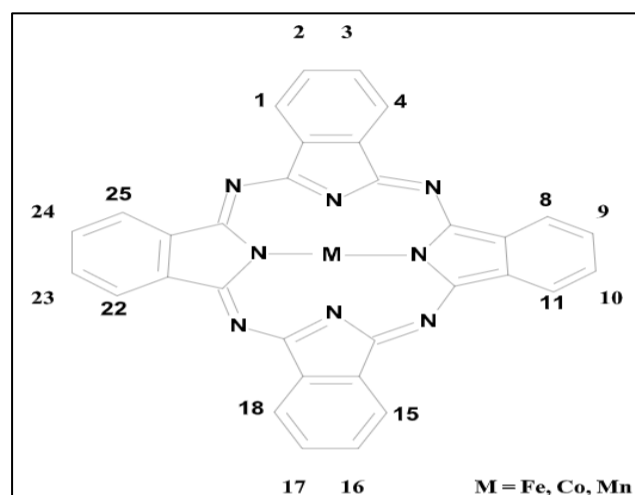


Fig 1 Molecular Structure of Metallophthalocyanines (MPc) with Numbering (Adopted from [4]).

The substitution in MPc complexes could be achieved either on the central metal ion or on the ring systems. The substituents on the ring could be mono, di, tetra or octa substituted groups. The substituent alters the properties of metallophthalocyanines, depending on their positions either

at the non-peripheral ( $\alpha$ ) or peripheral ( $\beta$ ) positions [5]. Also, the incorporation of different substituents, the positions of the substituents (either at  $\alpha$  or  $\beta$ - positions) and the electron-withdrawing or donating effect of different substituents affect their properties and enhances the solubility [6]. The incorporation of different metal at the MPcs core often influences the electrical, optical and magnetic properties of MPc [5], and they are excellent homogenous and heterogeneous catalysts for various applications. The flexibility, chemical, and thermal stability allow for their extensive application in the various areas of research, such as liquid crystal display devices [5], photovoltaic cells [7], fuel cells [8], semiconductor devices [9] and chemical sensors for various analytes. MPc is very stable and reusable electrocatalysts [10]. MPc with an octacarboxyphenoxy substituent group at the peripheral position and transition metals (Co, Fe, Mn) central metal substituents were employed in this work.

Fig 1 shows the synthetic routes for unsubstituted metallophthalocyanines. Diverse types of precursors are used for the synthesis of the phthalocyanines. The formation of metallophthalocyanines involves cyclotetramerization reaction. The reactions are carried out with the starting material such as (1) phthalonitrile, (2) phthalic acid, (3) phthalimide, (4) phthalic anhydride, (5) dibromobenzene, (6) 1, 3-diiminoisoindoline, and (7) Ocyanobenzamide. A high boiling solvent such as 1-pentanol and 1-octanol is used in the presence of catalysts. The catalyst could be Li or Na metal, 1, 8-Diazabicyclo (5.4.0) undec-7-ene (DBU) or 1, 5 – Diazabicyclo [4.3.0] non-5-ene (DBN).

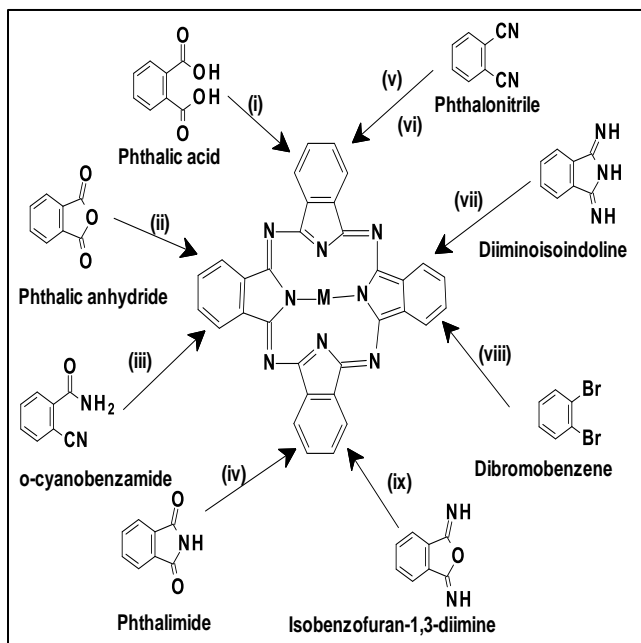


Fig 2 The Synthesis Routes of Metallophthalocyanines, Reaction and Conditions:(i) Urea, Metal Salt, Heat (ii)  $\text{NH}_3$ , Metal Salt, Solvent, Heat (iii) Metal Salt, Solvent,  $300^\circ\text{C}$  (iv) Formamide, Heat (v) ROH, Metal Salt, DBU,  $130^\circ\text{C}$  (vi) ROH, Solvent, Li Metal, Heat. (vii) Solvent, a Metal Salt (viii) CuCN, Heat (ix)  $\text{NH}_3$ , Metal Salt, Solvent, Heat.

### ➤ The Metallophthalocyanines Modified Electrode

Modification of electrodes with MPcs protects the electrode surfaces from chemical fouling, provides enhanced catalytic properties, improves sensitivity and selectivity.

The most widely reported method for MPcs immobilisation onto the electrode surface is via dip and drop dry method. Unfortunately, these methods suffer from high irreproducibility and poor stability [11]. Also, the MPcs layer thickness on the electrode surface cannot be controlled and film reproducibility is a major challenge. Agboola and Ozoemena [12] fabricated a sensitive epinephrine electrochemical sensor using gold electrode-prefunctionalized with cysteamine for the covalent immobilisation of octacarboxylcobalt phthalocyanine via amide bonding. The MPcs modifications via self-assembled monolayer technique (SAM) are not stable and have limited pH range applicability. The SAM layer has low shelf-life and therefore, has limited reliability. The stability of the MPc modified electrode, shelf-life, reliability and reproducibility of results depends on the immobilization technique employed.

In this work, the method targets immobilization technique that would be novel with high stability and longer shelf-life. This work therefore investigated the synthesis of octacarboxyphenoxy metallophthalocyanines and the covalent immobilization onto gold electrode. The gold electrode was chosen due to its excellent electrochemical activity. The stability of the octacarboxyphenoxy metallophthalocyanines complexes at the electrode surface at wider pH would be demonstrated. It is expected that the MPc would provide enhanced sensitivity and stability compared to SAM. The phenyldiazonium ( $\text{R-NO}_x$ ,  $\text{R-NH}_2$ ) formed an active aryl radical with the loss of nitrogen ( $\text{N}_2$ ).

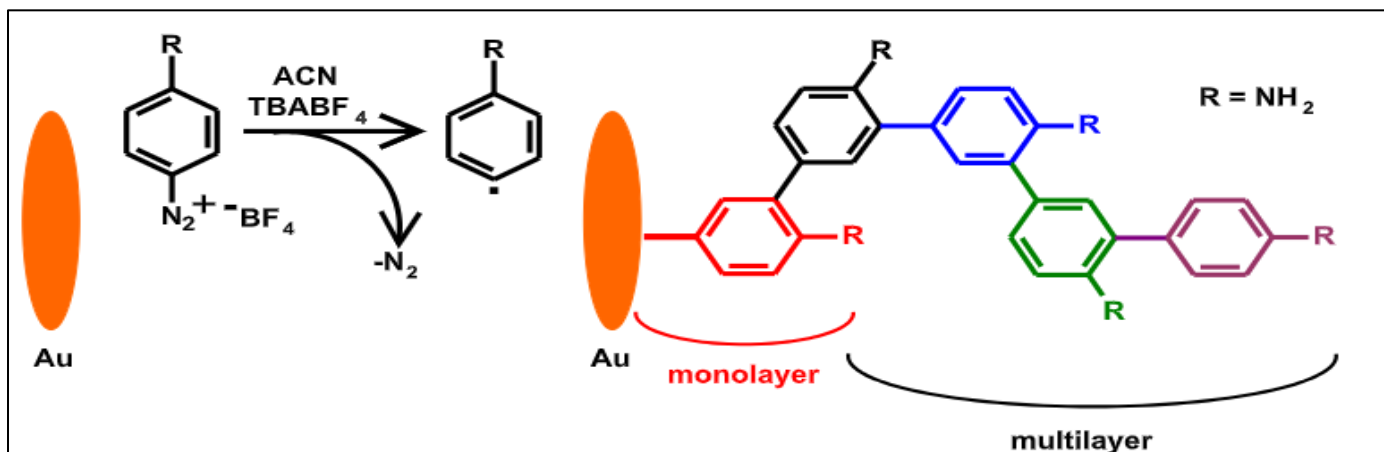


Fig 3 Electrochemical Grafting of Diazonium Salt onto Conductive Surface, for Mono or Multilayer Thin Film [10].

#### ➤ Amide coupling

Amide coupling formed a strong covalent bond between the carboxylic acid and amine functional groups. The process occurred through a nucleophilic substitution reaction. The COOH group is activated with EDC and NHS to form an amine-reactive succinimide ester as shown in Scheme 1.3. The mixture of the EDC/NHS was used to

activate the carboxyl group to obtain unstable and highly reactive NHS esters. In Scheme 1.3, the carboxylic acid reacted with the EDC to form an intermediate O-acrylisourea (urea derivative). NHS reacts with the O-acrylisourea to form NHS ester which conveniently reacted with the amine to form amide bond. The addition of NHS improved the efficiency of the amide formation [14].

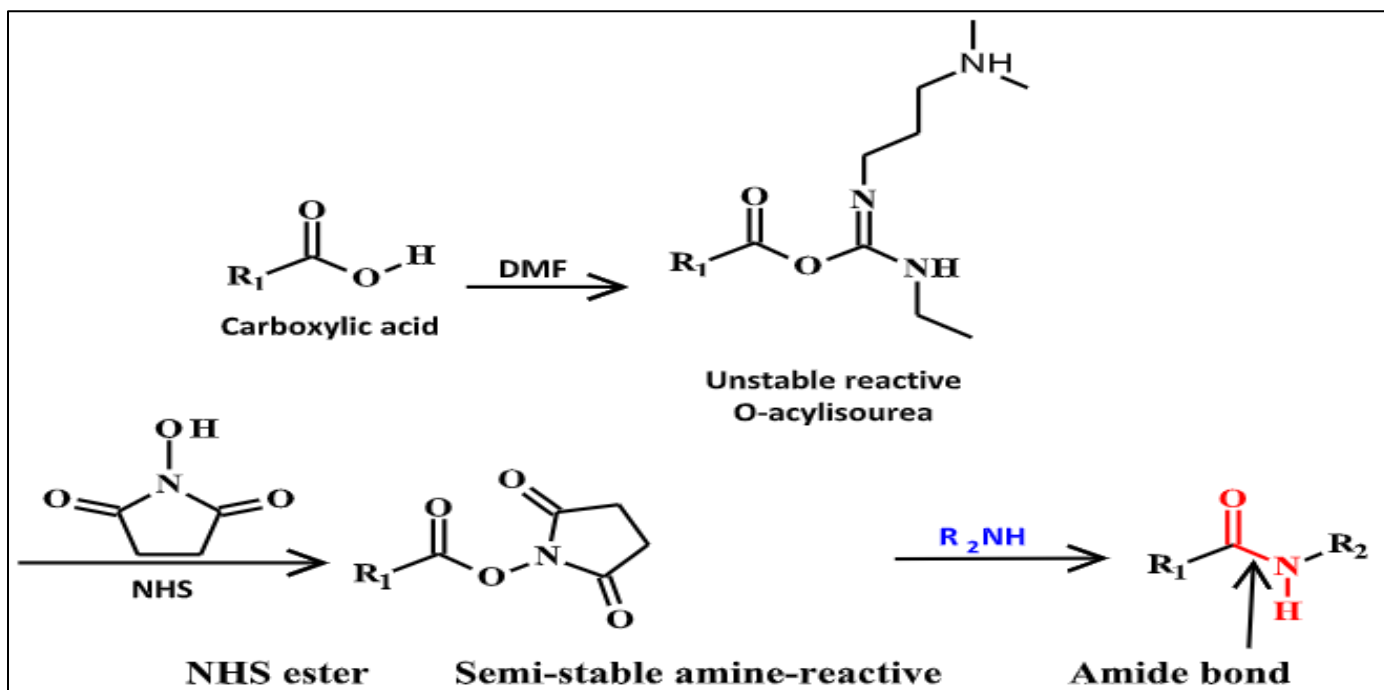


Fig 4 Amide Coupling Mechanism of Nucleophilic Substitution Reaction using EDC (1-Ethyl-3-(3-Dimethylaminopropyl)carbodiimide) and NHS (N-Hydroxysuccinimide). [15]

#### ➤ The Specific Objectives are to:

- Synthesise and characterise thoroughly octacarboxyphenoxy metallophthalocyanines complexes containing iron (Fe), cobalt (Co) and Mn (manganese) central metal ions;
- Covalently immobilise octacarboxyphenoxy metallophthalocyanines onto the gold electrode surface in a stable manner and study its electrochemical properties;
- Study the effect of pH of the modified phthalocyanines gold electrodes using negative and positively charged electroactive redox species

## II. METHODOLOGY

#### ➤ Materials and Reagents

Tetrabutylammonium tetrafluoroborate (TBABF<sub>4</sub>), 4-Nitroaniline (C<sub>6</sub>H<sub>6</sub>N<sub>2</sub>O<sub>2</sub>), 1,8-diazabicyclo-[5,4,0]-undec-7-ene (DBU), 1-ethyl-3-(3-dimethyl aminopropyl)

carbodiimide (EDC), N-hydroxysuccinimide (NHS), 4,5-dichlorophthalic acid, trifluoroacetic acid (TFA), 2,5-dihydroxybenzoic acid, 1-pentanol, and potassium ferrocyanide  $K_4[Fe(CN)_6]$  and potassium ferricyanide ( $K_3[Fe(CN)_6]$ ) were obtained from Sigma-Aldrich. Iron (II) chloride ( $FeCl_2$ ), manganese (II) acetate ( $Mn(OAc)_2$ ), acetonitrile (ACN), and potassium chloride (KCl), tetrahydrofuran (THF), ammonia hydroxide ( $NH_4OH$ ), Hydrochloric acid (HCl) were obtained from Minema. Potassium carbonate ( $K_2CO_3$ ), 25% ammonium hydroxide, sodium chloride (NaCl) and Silica Gel 60P F254 (Thin layer chromatography) were purchased from Merck. Potassium dihydrogen orthophosphate ( $KH_2PO_4$ ), dimethyl formamide (DMF), dimethyl sulfoxide (DMSO), and dipotassium hydrogen orthophosphate ( $K_2HPO_4$ ) and cobaltous acetate tetrahydrate ( $Co(OAc)_2 \cdot 4H_2O$ ) were purchased from Associated Chemical Enterprises (ACE). Hydrogen peroxide ( $H_2O_2$ ) and sodium hydroxide pellet were purchased from B & M Scientific. Absolute ethanol ( $C_2H_6O$ ) was purchased from SAARChem. Alumina powder was purchased from Allied High Tech. Silica Gel 60 (0.04-0.063 mm) for Column chromatography was obtained from Fluka. All other reagents were of analytical grade. Ultra-pure Milli-Q Water (18.2 M $\Omega$ . cm resistivity at 25°C) was obtained from the Milli – Q water system (Millipore Corp., Bedford, MA, USA) and was used to prepare all aqueous solutions.

Phosphate buffers saline (PBS) were prepared with ultrapure Millipore water, using appropriate amounts of  $KH_2PO_4$  (90.0 mg; 0.70 mmol),  $K_2HPO_4$  (1.63 g; 9.4 mmol), sodium chloride salts (8.0 g; 0.10 mmol) and KCl (20.0 mg; 0.30 mmol) for 100 ml. The quantities can be altered depending on the desired pH and the molarity. The activation buffer used was 2-(N- morpholine) ethanesulfonic acid (MES) buffer (10 mM, pH 6.5). The pH was adjusted using 0.10 M HCl, and 0.10 M NaOH. The gold and reference electrodes were purchased from BioAnalytical Systems Incorporation (BASi).

#### ➤ Experimental Techniques and Equipment

The electrochemical techniques employed in this study include cyclic voltammetry (CV), electrochemical impedance spectroscopy (EIS), and differential pulse voltammetry (DPV). The electrochemical measurements were conducted using an Autolab PGSTAT 302N equipped with Nova 1.10 software (FRA 32M). The conventional three-electrode electrochemical cell consists of gold working electrode (1.6 mm diameter), Ag|AgCl, 3M KCl reference electrode (6 mm diameter, 7.5 cm long with coral or frit at the tip) and platinum wire as counter electrode. The electrochemical impedance spectroscopy (EIS) measurements were carried out on the mirror polished bare, electrografted and modified electrode surfaces in 2.0 mM (1:1)  $K_3[Fe(CN)_6]$  and  $K_4[Fe(CN)_6]$  containing 0.10 M KCl. Metrohm 827 pH meter was used for the pH measurements. Hettich Zentrifugen MIKRO 220 Labotec was used for the centrifugation studies. Branson 1800 was used for ultrasonication studies.

#### ➤ Spectroscopic Characterisation of Synthesised Compounds and Complexes

##### • Fourier Transforms Infrared (FT-IR) Spectroscopy

The various complexes were characterized using FTIR data obtained from Bruker Alpha-model FT-IR Spectrometer (4000 - 650  $cm^{-1}$ ) or Perkin-Elmer Spectrum 100 FT-IR Spectrometer (4000 - 400  $cm^{-1}$ ) equipped with the diamond-attenuated total reflectance (ATR) sampling accessory. The two instruments were utilized interchangeable and there was no discrepancy for the data obtained. All measurements were recorded at room temperature. 100 Scans were taken for each interferogram at 4  $cm^{-1}$  resolutions. The background spectrum in the air was recorded and automatically subtracted from the sample spectrum by the appropriate software (Bruker OPUS 6.5 software) and (Perkin Elmer Spectrum One software).

##### • Nuclear Magnetic Resonance Spectroscopy (NMR)

NMR is a technique used for the determination of the structure of an organic compound and to confirm its purity. It involves the exposure of certain atomic nuclei notably  $^{13}C$ ,  $^1H$ ,  $^{19}F$  and  $^{31}P$  to an external magnetic field. The  $^1H$  chemically equivalent hydrogen will give signals in the  $^1H$  NMR. By integrating the area under the  $^1H$  signal, the number of chemically equivalent protons can be determined, hence revealing how many numbers of hydrogen atoms are present in a compound. In this study,  $^1H$  NMR was employed to elucidate the structure of the synthesised compounds and metallophthalocyanines and confirms the purity. The peaks were recorded in deuterated solvents of choice depending on the solubility of the compound or materials investigated. Solvents such as  $CDCl_3$  or  $DMSO-d_6$  were used and a Bruker 300MHz and 400MHz NMR spectrometer.

##### • Elemental Analysis

The elemental (CHN) and isotopic compositions in each of the prepared samples were conducted with a Vario-Elemental Microcube ELIII.

##### • Ultraviolet/Visible Absorption Spectroscopy (UV-Vis)

The spectra were recorded using a Perkin Elmer Lambda 25 Spectrometer and Multiskan sky Thermo Scientific UV equipment. The sample solution of 1 cm path length was used in the cuvette cell. The equipment measures the absorbance of ultraviolet or visible light by the sample. This could be either at a single wavelength or by performing a scan over a range of wavelengths in the spectrum. The radiation causes an electronic transition within the structure of a molecule or ion to exhibit absorption in the visible or ultraviolet region.

##### • Magnetic Circular Dichroism (MCD)

The MCD spectra were recorded with MCD Applied Photophysics Chirscan plus spectropolarimeter equipped with a permanent magnet, producing a magnetic field of 1 Tesla. The MCD spectra gives the differential absorption of left (lcp) and right (rcp) circularly polarized light. The light-induced in a sample by a strong magnetic field is oriented parallel to the direction of light propagation. It measures the

difference in intensity between left and right. The magnetic dipole moment was used to determine the intensity of MCD spectra, which gave better resolution than UV absorbance spectroscopy. The combination of UV-Vis and MCD spectroscopy provides direct information about the energies and degeneracies of the state that are responsible for the major spectral bands in the UV-Vis.

#### • Mass Spectroscopy (MS)

The mass spectra were recorded with Bruker AutoFLEX III smartdata beam MALDI/TOF (Matrix-assisted laser desorption/ionization/ time of flight) mass spectrometer. The matrix used in the positive ion mode was 2,5-dihydroxybenzoic acid. The technique ionizes chemical species and sorts the ions into a spectrum detector based on their mass-to-charge ratio. The matrix (0.10 mg, 0.60 mmol) was dissolved in 1 mL of acetonitrile:TFA (v:v 30:70). Other solvents that can be used for the preparation of the matrix are methanol, acetone, chloroform, and water. Metallophthalocyanine complexes (5.0  $\mu$ L) was mixed with matrix (20.0  $\mu$ L) and spotted on the equipment's stainless-steel plate and inserted into the instrument for analysis. The decoded results with relative intensity were interpreted.

#### ➤ Synthesis of Metallophthalocyanines

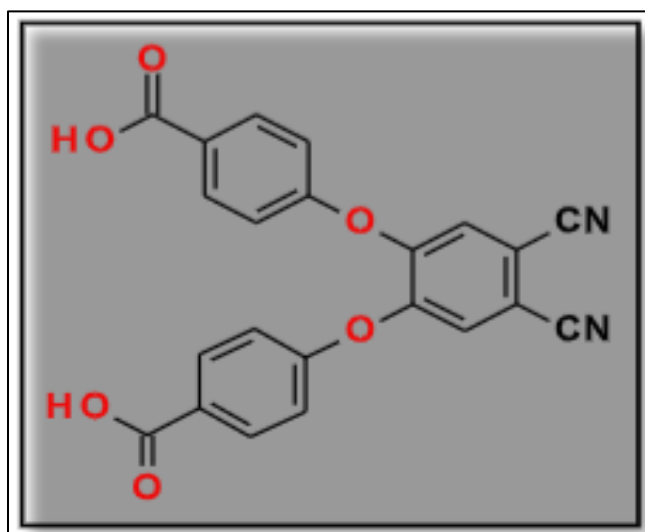


Fig 5 Synthesis of 4,5-di(4-Carboxyphenoxy) Phthalonitrile

The synthesis of 4, 5-di(carboxylphenoxy) phthalonitrile was carried out following the previously reported methods with slight modification [16]. A mixture of 4,5-dichlorophthalonitrile (0.5 g; 2.5mmol) and 4-hydroxybenzoic acid (1.0 g; 7.5 mmol) was stirred in dry DMSO (20.0 mL) at 50°C for 48 hours under Argon gas. Dried fine powdered of  $K_2CO_3$  (8 x (0.7 g; 5.0 mmol) and 8 x (10.0 mmol, 1.4 g) every 5 minutes was added. The reaction was cooled and added to ice. The precipitate formed was filtered off, washed with ice water, recrystallized with methanol and air-dried to obtain a white crystal of 4,5-di(4-carboxyphenoxy) phthalonitrile. Yield (0.8 g; 98.1%),  $^1H$ NMR (DMSO- $d_6$ )  $\delta$  (ppm); 7.21-7.18 (4H, d, Ar-H); 7.79 (2H, s, Ar-H); 8.01, 7.18 (4H, d, Ar - H), 8.44 (2H, s, (COOH) $_2$ ). FT-IR (ATR),  $\nu_{max}$  ( $cm^{-1}$ ): 3088

(O-H<sub>str</sub>) (and C-H<sub>str</sub>); 2234 (C≡N); 1679(C = O); 1082 (C-O-C) and 1285 (C-O<sub>str</sub>).

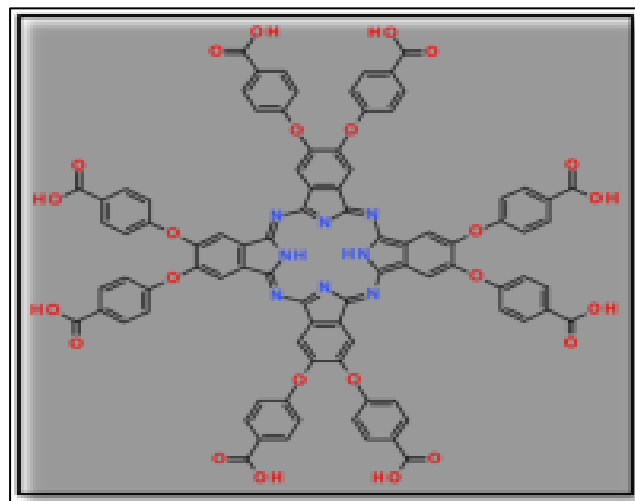


Fig 6 Synthesis of 2,3,9,10,16,17,23,24-Octacarboxyphenoxy Phthalocyanines (H<sub>2</sub>OcPhOPc).

A mixture of 4,5-di(4-carboxyphenoxy) phthalonitrile (0.30 g; 0.70 mmol), and lithium metal (40.0 mg) in 1-pentanol (3.0 mL) was refluxed under argon gas at 130°C for 16 hours. The green precipitate was obtained, and the lithium metal was removed from the precipitate with 50% aqueous acetic acid (1.0 mL). This was followed by successive purification under centrifugation using methanol and 1 M HCl. The product was dried and further purified with a silica gel packed column eluting with a mixture of methanol:THF (1:5). Yield 0.10 g (33%). FT-IR (ATR),  $\nu_{max}$  ( $cm^{-1}$ ); 3413 (N-H<sub>str</sub>), 1717 (C=O<sub>str</sub>), 1454 (C-H<sub>str</sub>), 1064 (C-O-C). UV-Vis (DMSO),  $\lambda_{max}$  nm ( $\epsilon$ ): 674 (3.43), 618 (4.30), 342 (4.90). MALDI-TOM MS (m/z): Calc.1602.01. Found 1601.52. [M<sup>+</sup>].

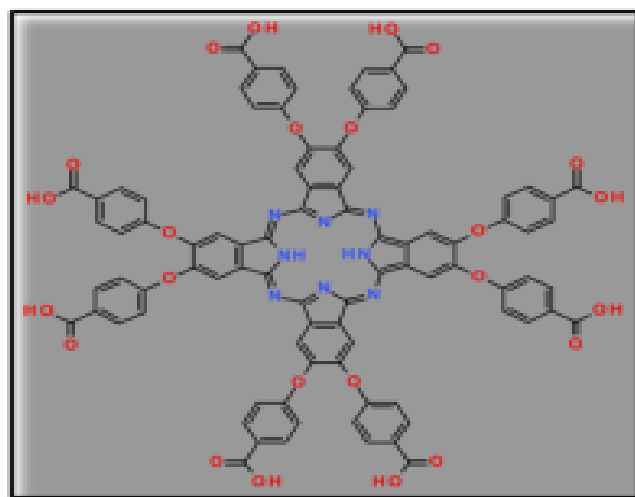


Fig 7 Synthesis of 2,3,9,10,16,17,23,24-Octacarboxyphenoxy Metallophthalocyanines (MOcPhPc),

The mixture of 4,5-di (4-carboxyphenoxy) phthalonitrile (0.3 g; 0.7 mmol), 1-pentanol (3.0 mL), DBU (0.04 mL, 0.3 mmol) and metal salt (0.4 mg; 2.0 mmol) and

refluxed under argon gas at 130°C for 16 hrs. After cooling to room temperature, the reaction mixture was precipitated by the addition of methanol, filtered and dried in air. The precipitate was treated with 1M HCl. The phthalocyanines were purified using silica gel column chromatography and methanol: THF (1:5) as eluent system.

The solvent was evaporated and the product was dried to yield FeOcPhOPc. Yield 60.0 mg (19%). FT-IR (ATR),  $\nu_{\max}$  (cm<sup>-1</sup>): 3264 (O-H), 2956 (Ar-C-H), 1714 (C=O), 1065 (C-O-C) and 1601 (Ar-C=C-C). UV-Vis (DMSO)  $\lambda_{\max}$  (nm) ( $\epsilon$ ): 631 nm (4.30). MALDI-TOF MS (m/z): Calc.1655.84, [M<sup>+</sup>]. Found 1653.71, [M - 2H<sup>+</sup>].

The metal salts used were iron (II) chloride (0.40 mg, 2.0 mmol), cobaltous acetate tetrahydrate (0.40 mg, 2.2 mmol) and manganese (II) acetate (0.40 mg; 2.3 mmol) to give three complexes.

- *CoOcPhOPc*

Yield 90.0 mg (30 %). FT-IR (ATR),  $\nu_{\max}$  (cm<sup>-1</sup>): 3256 (O-H), 2932 (C-H), 1717 (C=O), 1095 (C-O-C) and 1604 (Ar-C=C-C). UV-Vis (DMSO)  $\lambda_{\max}$  (nm) ( $\epsilon$ ): 661 (4.25), 338(2.54). MALDI-TOF MS (m/z): Calc.1654.93 [M<sup>+</sup>]. Found 1653.63 [M-H<sup>+</sup>].

- *Mn(OAc)OcPhOPc*

Yield 70.0 mg (23 %). FT-IR (ATR),  $\nu_{\max}$  (cm<sup>-1</sup>): 3382 (O-H), 1716 (C=O), 1083 (C-O-C) and 1601 (Ar-C=C-C). UV-Vis (DMSO)  $\lambda_{\max}$  (nm) ( $\epsilon$ ): 715 (4.27), 499 (4.17), 376 (1.56). MALDI-TOF MS (m/z): Calc.1656.93 [M<sup>+</sup>]. Found 1654.06 [M-2H<sup>+</sup>].

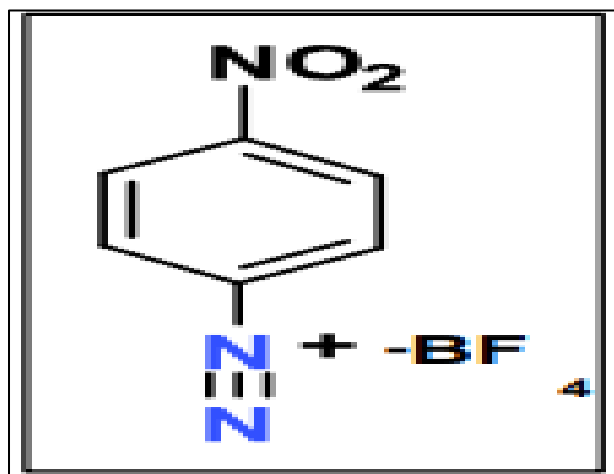


Fig 8 Synthesis of 4-Nitrobenzene Tetrafluoroborate Diazonium Salt

The synthesis of diazonium salt followed a reported method [66] with slight modification. Briefly, the 4-nitrobenzenediazonium tetrafluoroborate was synthesized by reacting 4-nitroaniline (1.04 g, 15.0 mmol) with HBF<sub>4</sub> (3.0 mL) and stirred for 15 minutes in an ice bath at -5°C. Ice cold solution of NaNO<sub>2</sub> (1.04 g, 30.0 mmol) was added drop wisely. The mixture was stirred vigorously for 40 minutes. The precipitate formed and was filtered, washed with petroleum ether and vacuum dried. The product was stored in the dark and frozen. Yield 0.84 g (82%). - FT-IR (ATR)

$\nu_{\max}$  (cm<sup>-1</sup>): 3381 (N-H), 3107 (Ar-CH), 2307 (N≡N), 1615 (C=C-C).

- *Electrode Modification with Diazonium and Metallophthalocyanines*

- *Electrode Pre-Treatments*

The gold electrode was first polished with aqueous slurries of alumina powder (< 2 μm) on a SiC emery paper (type 2400 grit). After which it was washed with a copious amount of Millipore water, and mirror-polished on a Buehler felt pad with various aqueous alumina slurries of 1 μm, 0.3 μm and 0.065 μm, respectively. The gold electrode was then subjected to ultrasonic vibration in absolute ethanol to remove residual alumina powder. The organic contaminant on the electrode surface was etched in a "Piranha" solution (1:3 (v/v) 30% H<sub>2</sub>O<sub>2</sub> and concentrated H<sub>2</sub>SO<sub>4</sub>) for about 2 minutes. Gold electrode was then rinsed with a copious amount of Milli-Q water and finally rinsed with absolute ethanol. The cleanliness was confirmed with cyclic voltammetry by subjecting the electrode to multiple cycle scans in 0.50 M H<sub>2</sub>SO<sub>4</sub>. The scanned potential was between -0.5 and 1.5 V (versus Ag|AgCl) at a scan rate of 50 mV/s until a reproducible scan was achieved.

- *Pre-Modification of Gold Electrode using Electrochemical Grafting Method*

The reductive electrodeposition of the synthesized 1.0 mM 4-nitrobenzene tetrafluoroborate diazonium salt (1.18 mg, 5.0 μmol) in ACN (5.0 mL) containing 0.1 M TBABF<sub>4</sub> (164.0 mg, 0.50 mol) was carried out. The cyclic voltammetry was run at four cycles at the potential range of + 0.40 V to - 0.40 V and at the fixed scan rate of 100 mV/s. Phenylamino formed on the gold surface (Au-PNO<sub>2</sub>). Au-PNO<sub>2</sub> was electrochemically reduced to phenylamino (Au-PA) group in aprotic solvent (ethanol/water) (1:9 v:v) containing 0.10 M KCl solution at the potential range between + 0.40 and -1.25 V at the fixed scan rate of 100 mV/s.

- *Immobilization of MOcPhOPc Complexes onto Au-PA to Yield Au-PA-MOcPhOPc*

The immobilization of MOcPhOPc was carried out after the electrografting process and following amide coupling. The phenylamino modified surface of the electrode (Au-PA) was dipped into DMF solution containing the EDC/NHS activated MOcPhOPc. EDC and NHS are coupling agent. A mixture of MOcPhOPc (5.0 mg, 6.0 μmol), NHS (57.5 mg, 49.7 mmol) and EDC (96.0 mg, 50.1 mmol) was dissolved in PBS pH 7.4 (5.0 ml) and allowed to react to form an active carbodiimide esters for 6 hours. The electrografted electrode (Au-PA) was immersed in the solution and kept for 6 hours. The active carbodiimide esters underwent a condensation reaction with the amino groups. The reaction resulted in the formation of amide bonds between the activated carboxylic acid functional groups of the phthalocyanine complexes and terminal amine functional groups on the electrode surface (Au-PA). The modified electrode was stored rinsed with phosphate buffer pH 4.0 to yield Au-PA-MOcPhOPc surfaces (M = Co, Fe, and Mn(OAc)).

### III. SYNTHESIS OF OCTA CARBOXY PHENOXY METALLOPHTHALOCYANINES

Figure 9 shows the schematic illustration of the synthesis of octacarboxyphenoxy metallophthalocyanines (4), (5) and (6). The first step involved the synthesis of 4,5-di(4-carboxyphenoxy) phthalonitrile (3). The synthesis of (3) involve nucleophilic aromatic substitution reaction between

4,5-dichlorophthalonitrile (1) and 4-hydroxybenzoic acid (2) in the presence of  $K_2CO_3$  as a base. The octacarboxyphenoxy phthalocyanine complexes (4), (5) and (6) were synthesised by cyclotetramerization of (3) in the presence of the corresponding metal salts (Fe, Mn, Co) using 1-pentanol as a refluxing solvent and catalytic amount of DBU refluxed at 200 °C.

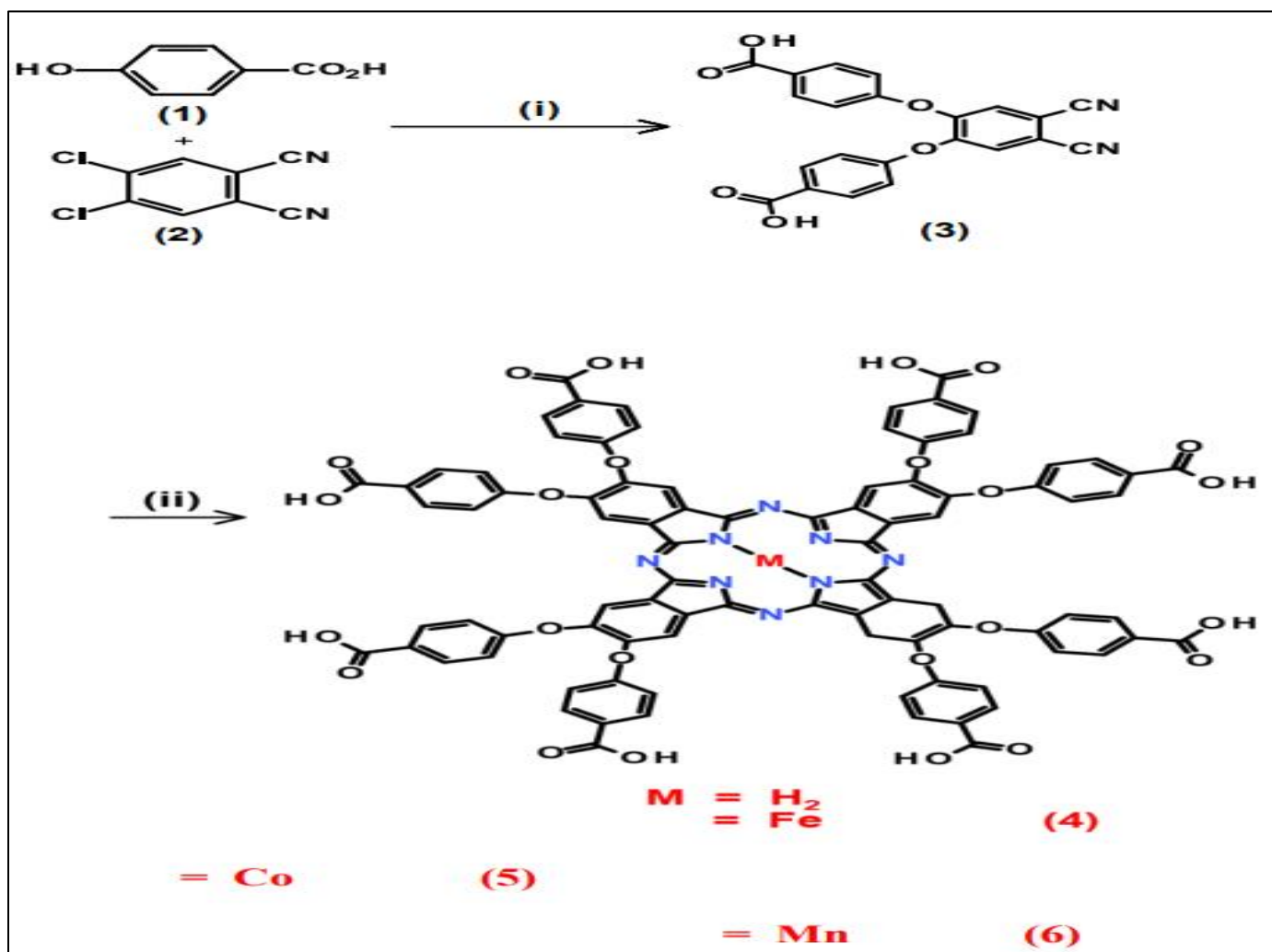


Fig 9 the Synthesis Route for Octacarboxyphenoxy Metallophthalocyanines (MOcPhOPc) Complexes. (i) Dry DMSO, Ar gas,  $K_2CO_3$ , 50 oC, 48 hrs; and (ii) 1pentanol, metal salt, DBU, 200 oC, 16 hrs.

#### ➤ Characterization of Complexes

##### • FT-IR Characterization of Metallophthalocyanines

Figure 10 shows the FT-IR spectra of (i) 4-hydroxybenzoic acid (1), (ii) 4,5dichlorophthalonitrile (2) and (iii) 4,5-di(4-carboxyphenoxy) phthalonitrile (3). The observed changes in the FTIR spectra shows the disappearance of hydroxyl (OH) stretch at  $3400\text{ cm}^{-1}$  for 4-hydroxybenzoic acid (1) and a shift of the carbonyl (C=O) from  $1669\text{ cm}^{-1}$  to  $1680\text{ cm}^{-1}$ . The disappearance of the C-Cl at  $829\text{ cm}^{-1}$  for 4,5-dichlorophthalonitrile (2) was observed. This was observed with an emergence of C-O ether stretch at  $1161\text{ cm}^{-1}$  confirming to formation of 4,5-di(4-carboxyphenoxy) phthalonitrile (3). The retention of the characteristic nitrile (C≡N) functional group at  $2234\text{ cm}^{-1}$

was observed. The FTIR results confirm the functional groups for the successful synthesis of 4,5-di(4-carboxyphenoxy) phthalonitrile (3).

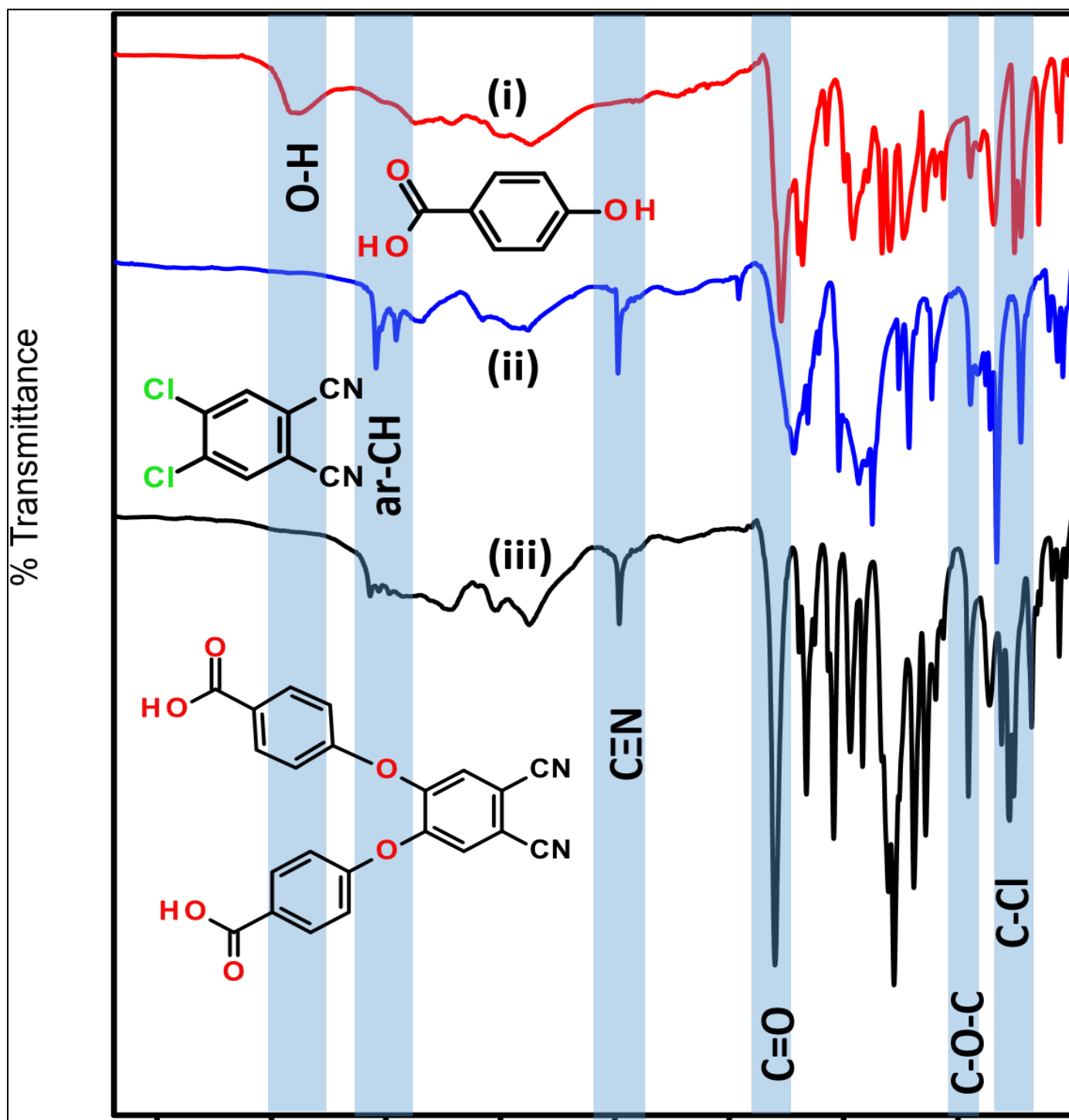


Fig 10 FT-IR Spectra of (i) 4-Hydroxybenzoic acid (1), (ii) 4,5-Dichloro Phthalonitrile (2) and (iii) 4,5-di(4-Carboxyphenoxy) Phthalonitrile (3). 3850 3450 3050 2650 2250 1850 1450 1050 650 Wavenumber ( $\text{cm}^{-1}$ )

Figure 11 shows the FT-IR spectra of (a) FeOcPhOPc (4), (b) CoOcPhOPc (5) and (c) Mn(OAc)OcPhOPc (6). The FTIR spectrum of FeOcPhOPc exhibited the OH stretch at  $3332 \text{ cm}^{-1}$ . The C=O stretch of the carboxylic acid was observed at  $1714 \text{ cm}^{-1}$ . The OH and C=O bands confirmed the presence of COOH of the carboxylphenoxy substituents on the FeOcPhOPc complex. The significant ar-C=C stretch from the aromatic ring was also observed at  $1596 \text{ cm}^{-1}$  and ar-CH was also observed at  $3080 \text{ cm}^{-1}$ . The disappearance of the characteristic C≡N peak of the precursor at  $2234 \text{ cm}^{-1}$  was also observed. The peak of the split C-O-C stretching

frequencies for the ether groups at  $1208 - 1161 \text{ cm}^{-1}$  was observed.

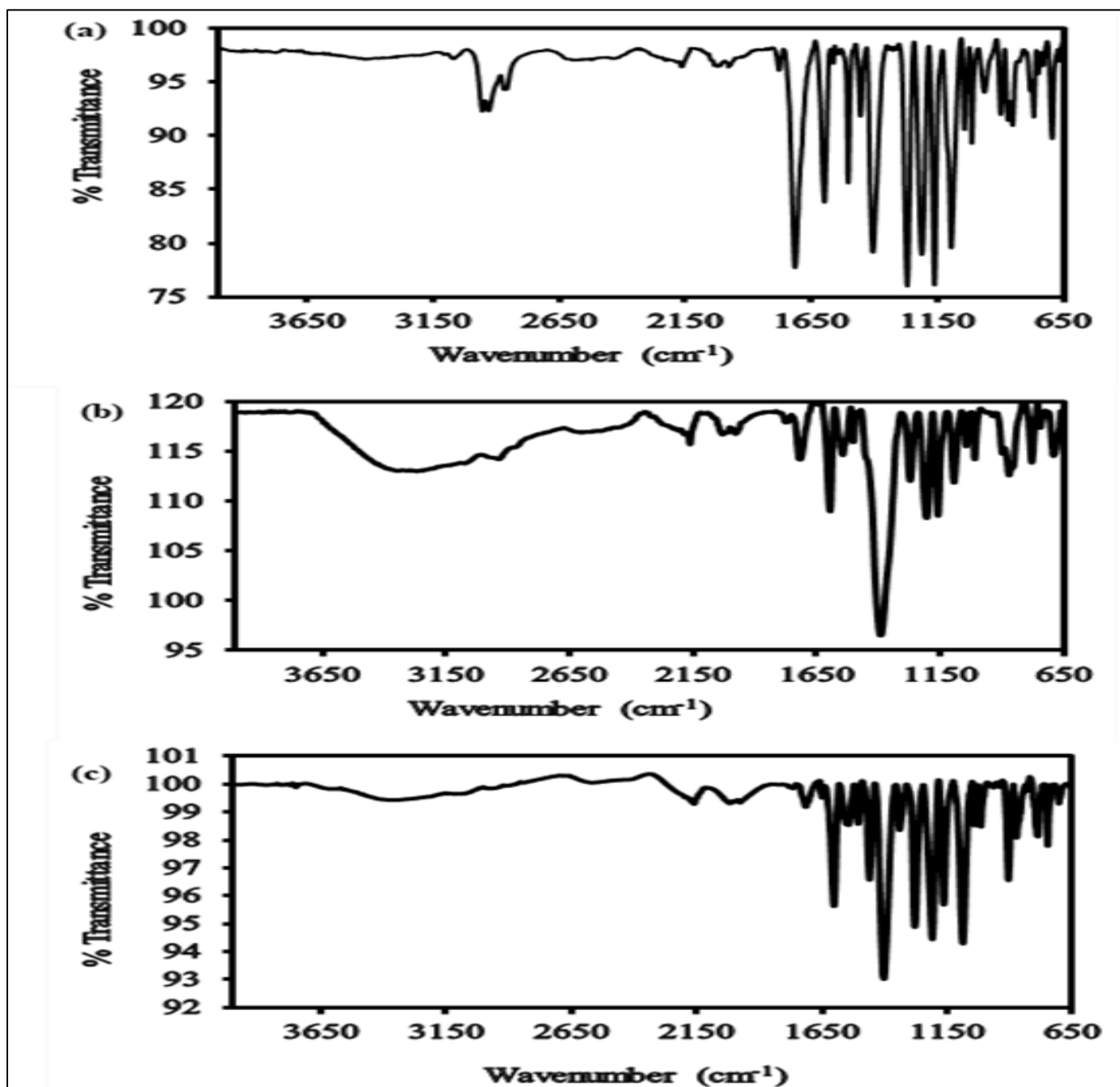


Fig 11 FT-IR Spectra of (a) FeOcPhOPc (4), (b) CoOcPhOPc (5), and (c) Mn(OAc)OcPhOPc (6).

In addition Figure 11 shows the FT-IR spectra of (b) CoOcPhOPc (5) and (c) Mn(OAc)OcPhOPc (6). The spectra for both complexes exhibited OH stretching peaks for the carboxylic acid group was observed at 3259 cm<sup>-1</sup> for CoOcPhOPc (5) and at 3382 cm<sup>-1</sup> for Mn(OAc)OcPhOPc (6). The C=O stretch of the carboxylic acid was observed at 1717 cm<sup>-1</sup> for CoOcPhOPc (5) and at 1716 cm<sup>-1</sup> for Mn(OAc)OcPhOPc (6). These confirmed the presence of COOH of the carboxylphenoxy substituents on the CoOcPhOPc (5) and Mn(OAc)OcPhOPc (6). The ar-CH peak at 2930 cm<sup>-1</sup> for the aromatic ring was observed. Similar to the FTIR for the FeOcPhOPc (4), the disappearance of the characteristic C≡N peak of the precursor at 2234 cm<sup>-1</sup> was also noticed for CoOcPhOPc (5) and Mn(OAc)OcPhOPc (6). The significant ar-CH peaks

for the aromatic ring was observed at 1598 cm<sup>-1</sup> and at 1597 cm<sup>-1</sup>, respectively for CoOcPhOPc (5) and Mn(OAc)OcPhOPc (6). The C-O stretch peak was observed at 1272 cm<sup>-1</sup>. The peak of the split C-O-C stretching frequencies for the ether groups was observed at 1206/1161 cm<sup>-1</sup> for CoOcPhOPc (5) and at 1207 – 1084 cm<sup>-1</sup> for Mn(OAc)OcPhOPc (6).

- Ultraviolet-visible (UV-Vis) characterization of MOcPhOPc

Figure 12 shows the UV-Vis absorption spectra of 12 nM of (a) FeOcPhOPc, (b) CoOcPhOPc, and (c) Mn(OAc)OcPhOPc complexes in DMSO. The electronic ground state absorption spectra of complexes FeOcPhOPc

(4), CoOcPhOPc (5), and Mn(OAc)OcPhOPc (6) showed monomeric behaviour with a single Q-band at 631 nm, 661 nm and 715 nm respectively. The single Q-bands are characteristics of metal containing phthalocyanines with degenerate  $e_g$  orbital. This reflects the transitions between the highest occupied molecular orbital (HOMO) to the lowest unoccupied molecular orbital (LUMO) of the delocalized phthalocyanines. The red shift in the position of the Q-band of the Mn(OAc)OcPhOPc complex relative to FeOcPhOPc and CoOcPhOPc could be attributed to increase in oxidation state Mn(III) and a decrease in the energy band gap between the HOMO and the LUMO orbitals after the insertion of the transition metal. The B-band of the complexes (5) and (6) were observed at 338 nm and 376 nm; respectively. The B-bands are a resultant transition from the  $b_{2u}$  and  $a_{2u}$  transitions to  $e_g$ . For the Mn(OAc)OcPhOPc (6) there was an additional band at 498 nm due to the metal-to-ligand (MLCT) or ligand-to-metal (LMCT) charge transfer. These are due to the Mn metal orbitals lying between the HOMO and LUMO orbital of the phthalocyanine ring allowing for transitions from the Pc ligand to metal orbitals or from metal orbitals to Pc ligand.

The molecular interaction of the complex monomers could result in aggregation, thereby causing a decrease in intensity and broadening of Q-band. The aggregation behaviour of the complexes was further investigated with different concentrations of complexes (4), (5), and (6) in DMSO. Figure 13 shows the UV-Vis absorption spectra of different concentrations of (a) FeOcPhOPc, (b) CoOcPhOPc, and (c) Mn(OAc)OcPhOPc complexes in DMSO. The UV-Vis of complex (4) in Figure 13 (a) showed a broad Q-band even at lower concentrations, which suggested that the complex (4) aggregates in DMSO. The aggregation behaviour of complex (4) could be attributed to the formation of  $\pi$ - $\pi$  interaction and could account for the absence of the B-band in complex (4). The UV-Vis spectra of complexes (5) and (6) in Figure 3.4 (b) and (c) showed a sharp Q-band even at higher concentrations up to 15.1 nM. This confirmed that complexes (5) and (6) are monomeric and no aggregation was observed in DMSO.

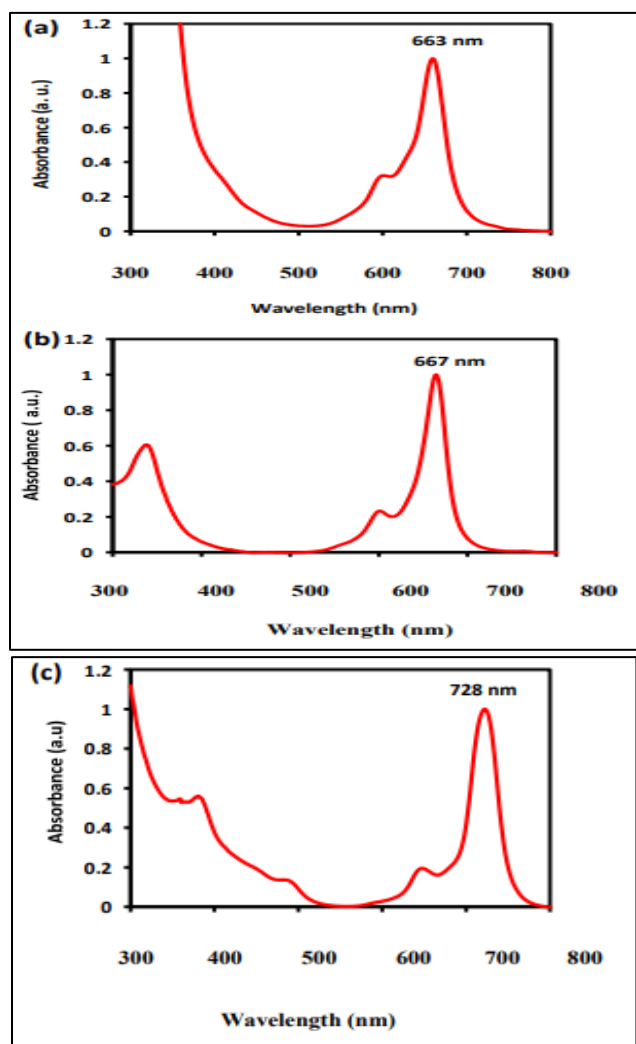


Fig 12 UV-Vis Absorption spectra of 12 nM of (a) FeOcPhOPc, (b) CoOcPhOPc, and (c) Mn(OAc)OcPhOPc Complexes in DMSO.

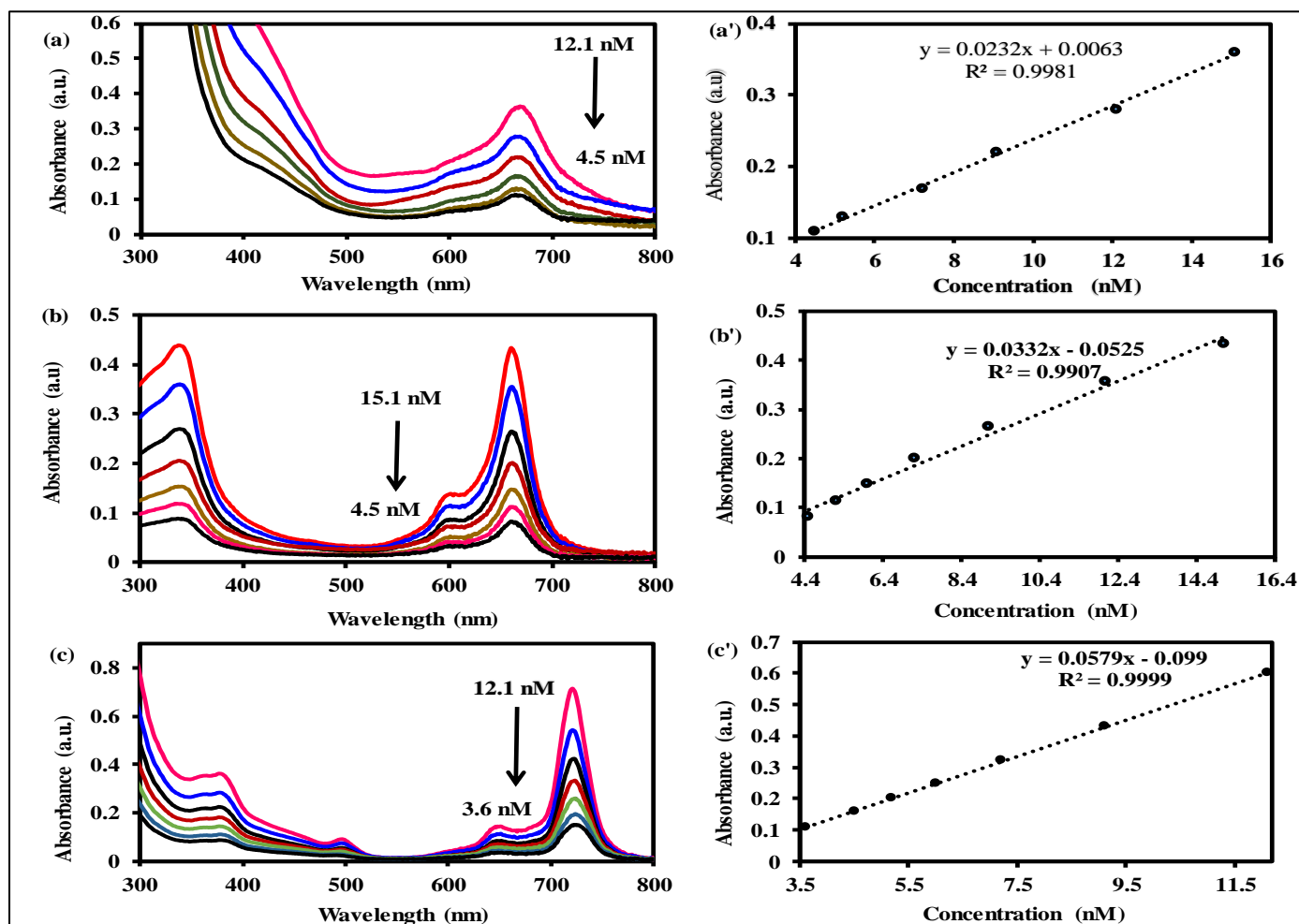


Fig 13 Aggregation studies relationship between absorbance for different concentrations of (a) FeOcPhOPc, (b) CoOcPhOPc, (c) Mn(OAc)OcPhOPc complexes in DMSO.

- Magnetic circular dichroism (MCD) characterization of complexes

Figure 14 shows the MCD and UV-Vis spectra of 12 nM (a) H<sub>2</sub>OcPhOPc, (b) FeOcPhOPc, (c) CoOcPhOPc, and (d) Mn(OAc)OcPhOPc. The split peaks in the H<sub>2</sub>OcPhOPc MCD in Figure 3.5 (a) confirmed the Faraday B terms, which correspond to the two separate peaks of the Q-band in the UV-Vis absorption spectrum of H<sub>2</sub>OcPhOPc. This is normally expected for metal-free phthalocyanines. The Faraday B term arises from the effects of Zeeman splitting of the zero-field states through magnetic dipole moments transitions [17]. The MCD transition for FeOcPhOPc (4) in Figure 3.5 (b) indicated a pseudo -Faraday A term. It arises from the  $\pi \rightarrow \pi^*$  transition in a degenerate state. The energy splitting transition is small, the MCD curve observed appear like a Faraday A terms but differs. The absorbance of the MCD band at 631 (-)  $\text{cm}^{-1}$  corresponds to the absorbance of the UV-Vis Q-band at 631 nm. The absorbance of the UV-Vis and MCD for CoOcPhOPc (5) at room temperature in Figure 3.5 (c) indicated a Faraday A terms. The peaks correspond to the absorption peaks, which confirmed the D<sub>4h</sub> symmetry. The MCD observed Faraday A terms at 661 and 600 (-)  $\text{cm}^{-1}$  corresponding to the Q-bands at 661 nm and 600 nm. The band at 339 (-)  $\text{cm}^{-1}$  which corresponds to 338 nm (Soret band) of the UV-Vis bands at room temperature.

It confirmed the D<sub>4h</sub> symmetry for complex (5). The MCD spectrum of Mn(OAc)OcPhOPc (6) in Figure 3.5 (d) clearly showed a single Q band corresponding to a Faraday A term. The peaks correspond to the absorption peaks, which confirmed the D<sub>4h</sub> symmetry. MCD spectrum of the  $\pi \rightarrow \pi^*$  transitions is observed at 718 (-)  $\text{cm}^{-1}$  which corresponds to 715 nm (Q-band). Ligand-to-metal charge transfer (LMCT) and metal-to-ligand charge transfer (MLCT) at 496  $\text{cm}^{-1}$  correspond to 498 nm. The B band observed at 376 nm corresponds to 374 (-)  $\text{cm}^{-1}$  in the MCD spectra. This confirmed the D<sub>4h</sub> symmetry for complex (6). This allowed the identification of specific transitions that may have overlapped in the absorption spectra.

- Mass Spectrometry Characterization of MPC

The octacarboxyphenoxy metallophthalocyanines complexes were characterized using MALDI-TOF mass spectrometer. Table 1 summarized the theoretical and experimental molecular mass of the synthesised complexes. The mass spectra for FeOcPhOPc showed a molecular ion peak at  $m/z = 1653.71$  [M-2H]<sup>+</sup>, CoOcPhOPc peaks at 1661.67 [M+3H]<sup>+</sup> and Mn(OAc)OcPhOPc peak  $m/z$  at 1653.90 [M-H]<sup>+</sup>. The mass spectroscopy results shown in Table 1 confirmed the successful formation of the complexes.

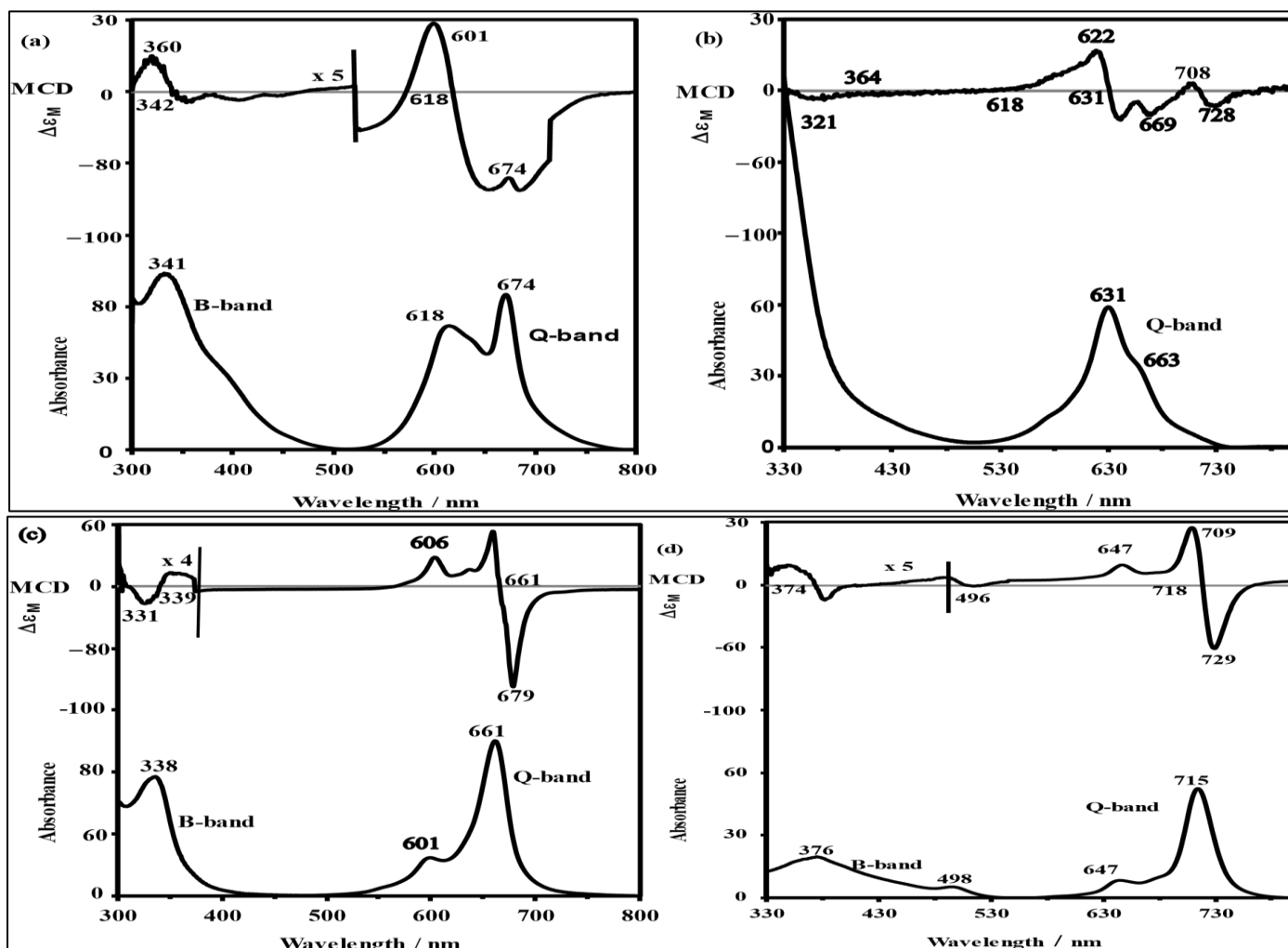


Fig 14 MCD and UV-Vis spectra of 12 nM of (a) H<sub>2</sub>OcPhOPc (b) FeOcPhOPc (c) CoOcPhOPc and (d) Mn(OAc)OcPhOPc in THF.

Table 1 Showing Summary of Characterization of the Complexes with FT-IR, UV-Vis, MCD, MS, and Elemental Analysis.

Complexes	FT-IR (cm <sup>-1</sup> )		UV-Vis (nm)		MS (m/z)		Elemental					
	Groups	Wavenumber	Wavelength (λ, nm), log ε	Assigned bands	Expected	Found	Expected (%)			Found (%)		
							C	H	N	C	H	N
<b>FeOcPhOPc</b>	OH	3332	663	Q band	1656.2131	1653.71	59.45	3.67	6.86	59.9	4.2	8.1
	arCH	3020	608	Vibronic band	[M] <sup>+</sup>	[M-2H] <sup>+</sup>						
	C=O	1714										
	ar-C=C	1596										
	C-O-C	1208-1161										
<b>CoOcPhPc</b>	OH	3259	667	Q band	1659.2113	1661.67	63.8	3.1	6.7	49.1	1.5	7.4
	C=O	1717	607	Vibronic band	[M] <sup>+</sup>	[M+3H] <sup>+</sup>						
	ar-CH	2930										
	arC=C	1598										
	C-O	1272	343	B (Soret) band								
	C-O-C	1206-1161										
<b>Mn(OAc)OcPhOPc</b>	OH	3382	728	Q band	1655.2162	1653.70	63.9	3.1	6.7	59.2	3.7	5.3
	arCH	3020			[M] <sup>+</sup>	[M-2H] <sup>+</sup>						
	C=O	1716	655	Vibronic band								
	ar-C=C	1597	495	MLCT/LMCT								
	C-O-C	1207-1084	386	B (Soret) band								

➤ *Electrode Modification and Surface Characterisation*

Figure 15 shows the schematic illustration of the immobilisation of the octacarboxyphenoxy metallophthalocyanines complexes (4), (5) and (6) onto the gold electrode surface. The first step involves the formation of a thin-film of phenylamino functional group on the gold electrode, represented as Au-PA. This was achieved via electrochemical grafting of 1.0 mmol. L<sup>-1</sup> 4-nitrobenzene tetrafluoroborate diazonium salt in a solution of 0.10 mol.L<sup>-1</sup> TBABF<sub>4</sub>. This process involves the electrochemically reduction of 4-nitrobenzene tetrafluoroborate diazonium to form phenylnitro radical. Upon scanning to more negative potential, the phenylnitro radical is then grafted onto the gold electrode surface. The phenylnitro modified gold electrode surface was represented as Au-PNO<sub>2</sub>. Subsequently, the Au-PNO<sub>2</sub> surface was electrochemically reduced by cycling between +0.25 to -1.25 V vs Ag|AgCl in (1:10 by v: v) ethanol/water mixture containing 0.10 mol.L<sup>-1</sup>

KCl. The Au-PNO<sub>2</sub> surface was reduced to the phenylamino group functionalized gold surface (Au-PA). The Au-PA have terminal NH<sub>2</sub> group.

The immobilisation of the synthesised FeOcPhOPc (4), CoOcPhOPc (5), and Mn(OAc)OcPhOPc (6) onto the Au-PA electrode was achieved via EDC/NHS carbodiimide crosslinking reaction. The crosslinking reaction involves the activation of the terminal carboxylic acid groups of the complexes with EDC and NHS to form is amine reactive succinimide ester groups (semi-stable NHS-activated complexes). The NHS-activated complex reacts with the amine groups of the Au-PA electrode via amide bond formation. A similar immobilisation process was used for covalent attachment of all the complexes onto the gold electrode surface to yield, Au-PA-CoOcPhOPc, Au-PA-FeOcPhOPc and Au-PA-MnOcPhOPc.

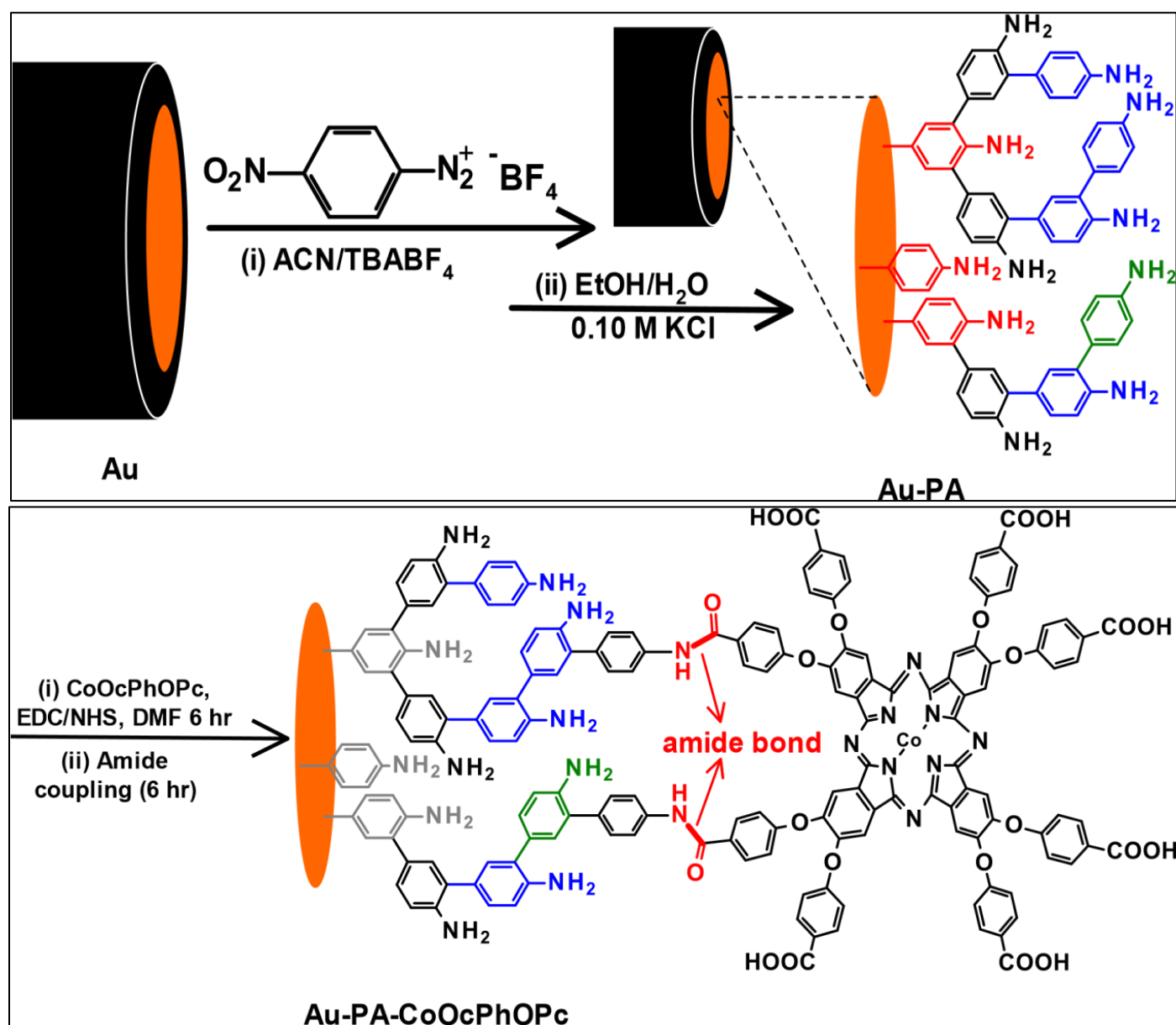


Fig 15 Procedure for the electrochemical grafting and immobilisation of CoOcPhOPc onto gold electrode surface premodified with phenylamine represented as Au-PA-CoOcPhOPc. Similar procedure was used for the immobilisation of FeOcPhOPc (Au-PA-FeOcPhOPc) and Mn(OAc)OcPhOPc (Au-PA-Mn(OAc)OcPhOPc).

➤ *Electrografting and Characterization of Au, Au-PA and Au-PA-CoOcPhOPc surfaces*

• *Cyclic Voltammetry of Modification of Electrode with Phenylamino (Au-PA)*

Figure 125 shows the cyclic voltammograms for (a) electrochemical reduction of 4-nitrobenzene diazonium salt, and (b) electrochemical reduction of phenylnitro group to form phenylamino group. The first scan in the voltammograms in Figure 4.1 (a)(i) showed a cathodic peak at 0.31 V. This reduction peak corresponds to the electrochemical reduction of the diazonium and the formation of the phenylnitro radical with loss of  $N_2$ . The radical attached to the gold electrode and formed a thin film of phenylnitro (Au-PNO<sub>2</sub>) on the electrode surface when the potential is scanned to the potential that is more negative. The cathodic peak disappeared during the subsequent scans due to the grafting of the radical onto the electrode surface. This confirms the formation of phenylnitro layer on the Au electrode surface. The use of three CV scans was employed to achieve a thin of monolayer or few multilayers. The formation of a monolayer is idealistic but not achievable

even though some reports have claimed the formation of a monolayer [18]. It is possible to form a thin multilayer film and a study of distinct number of layer deposition is ideal but not a subject of this work.

Figure 15 shows the cyclic voltammograms for electrochemical reduction of phenylnitro to form phenylamino groups. The first scan in the voltammograms in Figure 4.1 (b)(i) showed intense cathodic peak at -0.92 V (labelled II). This cathodic peak corresponds to the reduction of the phenylnitro group (PNO<sub>2</sub>) to phenylhydroxylamine group (PHA). The PHA oxidizes to phenylnitroso group and the CV in Figure 4.1 (b)(ii) showed an oxidation peak at -0.27 V (labelled III). The peak at -0.42 V in Figure 15 (b) (iii) was due to the reduction of PHA to phenylamino group (PA) thus the formation of Au-PA. On subsequent scans, the reduction peak at -0.92 V disappeared, confirming the conversion of the phenylnitro groups to phenylamino group. The peak at -0.92 V was preceded by a peak at -0.63 V (labelled I) attributed to the reduction of the physisorbed phenylnitro on the phenylnitro modified surface.

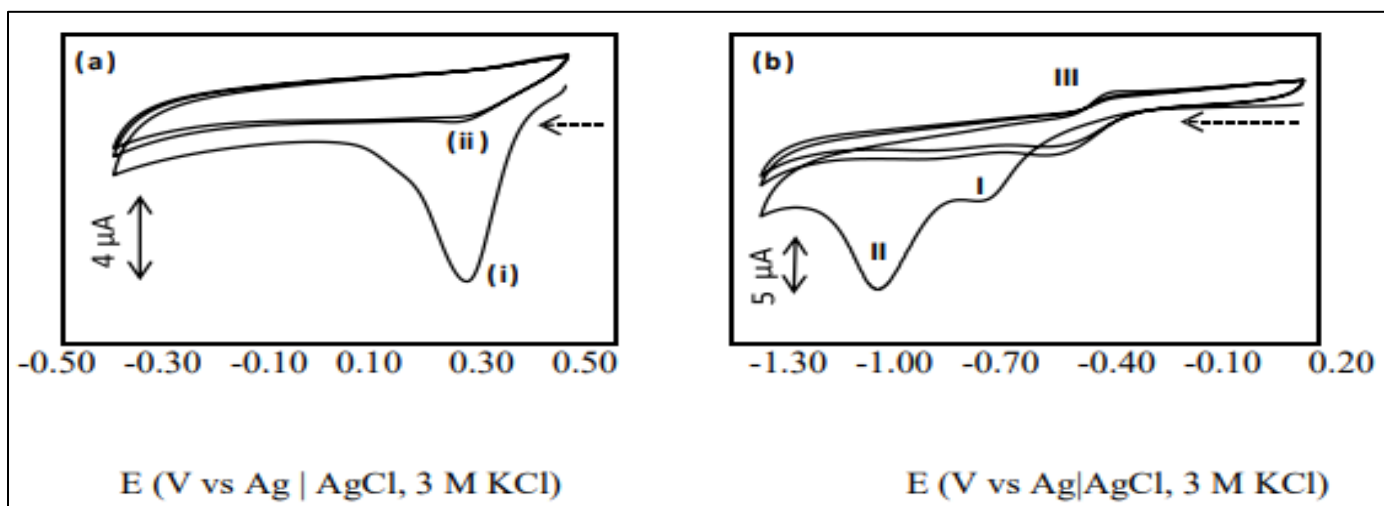


Fig 16 Cyclic voltammograms of (a) the electroreduction and grafting of phenylnitro from 1.0 mM 4-nitrobenzene diazonium salt tetrafluoroborate in ACN containing 0.10 M TBABF<sub>4</sub> in 3 cycles and (b) reduction of NO<sub>2</sub> to NH<sub>2</sub> in ethanol/water (1:9) solution containing 0.10 M KCl. Scan rate 100 mV.s<sup>-1</sup>.

• *Cyclic Voltammetry and Electrochemical Impedance Spectroscopy Studies*

Figure 17 shows the cyclic voltammograms (CVs) and the electrochemical impedance spectroscopy (EIS) of the (i) bare Au, (ii) Au-PA and (iii) Au-PA-CoOcPhOPc in (a) 2.0 mmol.L<sup>-1</sup> K<sub>3</sub>/K<sub>4</sub>[Fe(CN)<sub>6</sub>] and (b) 2 mmol.L<sup>-1</sup> [Ru(NH<sub>3</sub>)<sub>6</sub>] containing 0.10 mol.L<sup>-1</sup> KCl at a scan rate of 50 mV.s<sup>-1</sup>. The CV of the bare Au electrode in K<sub>3</sub>/K<sub>4</sub>[Fe(CN)<sub>6</sub>] in Figure 4.2 (a) (i) showed Fe<sup>II</sup>/Fe<sup>III</sup> reversible redox couple of [Fe(CN)<sub>6</sub>]<sup>3-/4-</sup> with a peak-to-peak separation ( $\Delta E$ ) of  $73 \pm 4.4$  mV. The CV of the Au-PA electrode in Figure 4.2 (ii) showed a decrease in peak current when compared to the bare Au electrode. The cathodic peak shifted to higher potential and the anodic peak was not observed. This showed that the PA-layer passivates the Au surface and blocks electron transfer process. The CV of the Au-PA-CoOcPhOPc showed restoration (to some extent) of the Fe<sup>II</sup>/Fe<sup>III</sup> reversible redox couple of [Fe(CN)<sub>6</sub>]<sup>3-/4-</sup>. At AuPA-

CoOcPhOPc, the  $\Delta E$  was  $154 \pm 4.53$  mV. The restoration of the redox process at the AuPA-CoOcPhOPc surface was attributed to the electrocatalytic properties of CoOcPhOPc towards [Fe(CN)<sub>6</sub>]<sup>3-/4-</sup> redox couple. The anodic and cathodic current at the Au-PACoOcPhOPc were very small compared to the bare Au surface but much higher compared to Au-PA surface. The slow electrode kinetics results from the slight repulsive effect of the negatively charged carboxyl (COO<sup>-</sup>) groups of Au-PA-CoOcPhOPc or delayed electron transfer due to the Au-PA thin film. Both these phenomena are possible, the pH studies will be investigated later. The restoration of the Fe<sup>II</sup>/Fe<sup>III</sup> redox couple due to [Fe(CN)<sub>6</sub>]<sup>3-/4-</sup> was observed for the Au-PA-FeOcPhOPc and Au-PA-Mn(OAc)OcPhOPc with the peak to peak separation of  $127 \pm 2.52$  mV and  $188 \pm 2.56$  mV respectively. The restoration of the redox couple is due to the observed phenomena for the Au-PA-CoOcPhOPc as discussed above.

The redox properties of the bare and modified electrodes were studied with a positive redox probe using Ruthenium hexamine,  $[\text{Ru}(\text{NH}_3)_6]^{2+/3+}$ , solution. The cyclic voltammograms of the bare Au electrode in  $2.0 \text{ mmol.L}^{-1}$   $\text{Ru}(\text{NH}_3)_6$  containing  $0.10 \text{ M}$  KCl are shown in Figure 17 (b)(i). A characteristic  $[\text{Ru}(\text{NH}_3)_6]^{2+/3+}$  redox couple with an anodic potential at  $170 \text{ mV}$  and a cathodic peak at  $-260 \text{ mV}$  was observed. The peak-to-peak separation ( $\Delta E$ ) was  $90 \text{ mV}$ . The CV of the Au-PA in the  $[\text{Ru}(\text{NH}_3)_6]$  solution in Figure 17 (b)(ii) showed a complete blockage of the electrode surface and no observable cathodic or anodic peak observed. This was attributed to the thin PA layer coating the gold electrode surface. The CV of the Au-PACoOcPhOPc in Figure 4.2 (b)(iii) showed restoration of  $[\text{Ru}(\text{NH}_3)_6]^{2+/3+}$

redox couple with an increase in cathodic and anodic peak currents. The immobilization of CoOcPhOPc to form Au-PA-CoOcPhOPc onto the Au-PA layer was confirmed and the catalytic nature of the CoOcPhOPc also catalyzed the  $[\text{Ru}(\text{NH}_3)_6]^{2+/3+}$  redox couple. The anodic and cathodic peaks shifted to lower potential in comparison to the bare Au surface with a  $\Delta E$  of  $92 \text{ mV}$ . The effect resulted from the electrostatic attraction between the positively charged  $[\text{Ru}(\text{NH}_3)_6]^{2+/3+}$  and the negative charge carboxylic acid ( $\text{COO}^-$ ) of the Au-PA-CoOcPhOPc. Similar results in term of the increase in anodic and cathodic currents were observed for Au-PA-FeOcPhOPc and AuPA-Mn(OAc)OcPhOPc.

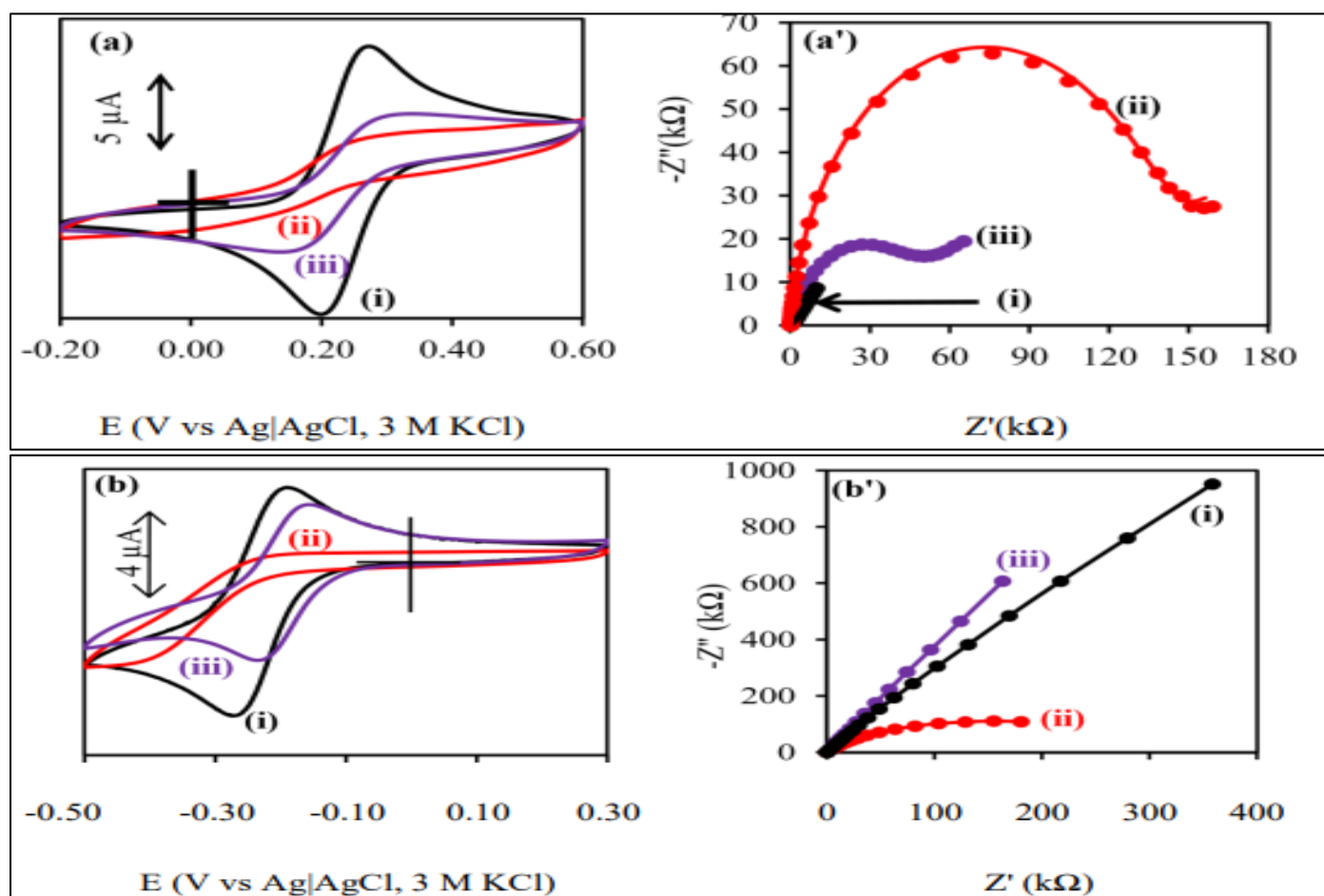


Fig 17 CV and EIS of (i) bare Au, (ii) Au-PA and (iii) Au-PA-CoOcPhOPc in (a)  $2.0 \text{ mM}$   $\text{K}_3/\text{K}_4[\text{Fe}(\text{CN})_6]$  and (b)  $2.0 \text{ mM}$   $\text{Ru}(\text{NH}_3)_6$  containing  $0.10 \text{ M}$  KCl. Scan rate of  $50 \text{ mV.s}^{-1}$ .

The  $\Delta E$  were summarized in Table 1. Furthermore, the electrochemical impedance characteristics of the modified surfaces were recorded to investigate the electron transfer properties on modified gold surfaces. Figure 17 (a') show the Nyquist plot of (i) Au, (ii) AuPA and (iii) Au-PA-MOcPhPc in  $2.0 \text{ mmol.L}^{-1}$   $\text{K}_3/\text{K}_4[\text{Fe}(\text{CN})_6]$  containing  $0.10 \text{ mol.L}^{-1}$  KCl. The charged transfer resistance ( $R_{CT}$ ) for the bare Au electrode was  $0.67 \text{ k}\Omega.\text{cm}^{-2}$ . The  $R_{CT}$  increased significantly to  $139 \text{ k}\Omega.\text{cm}^{-2}$  and attributed to the inhibition of electron transfer process after the formation of the Au-PA thin film. The Nyquist plot of Au-PA-MOcPhPc in Figure 17 (a') (iii) showed a decrease in the  $R_{CT}$  from  $139 \text{ k}\Omega.\text{cm}^{-2}$  for Au-PA to  $9.01 \text{ k}\Omega.\text{cm}^{-2}$  for Au-PA-CoOcPhOPc. The

decrease was due to the conductivity of CoOcPhOPc. For the other MPc complex modified electrodes similar trends were observed and  $R_{CT}$  decreased to  $25.10 \text{ k}\Omega.\text{cm}^{-2}$  for Au-PA-Mn(OAc)OcPhOPc and  $27.70 \text{ k}\Omega.\text{cm}^{-2}$  for Au-PA-FeOcPhOPc. The impedance data was accepted when the error (% error) of all the circuit elements was less than 5% and are summarized in Table 1. The Nyquist plot of the (i) bare Au, (ii) Au-PA, and (iii) Au-PA-CoOcPhOPc in  $2.0 \text{ mmol.L}^{-1}$   $\text{Ru}(\text{NH}_3)_6$  solution are shown in Figure 17(b'). The Nyquist plot of the bare Au in  $\text{Ru}(\text{NH}_3)_6$  in Figure 17 (b') (i) had  $R_{CT}$  of  $0.010 \text{ k}\Omega.\text{cm}^{-2}$ . The  $R_{CT}$  for the Au-PA increased to  $0.26 \text{ k}\Omega.\text{cm}^{-2}$  due to the passivation of the PA thin film after formation of Au-PA. On Au-PA-CoOcPhOPc,

the  $R_{CT}$  decreased to  $0.17 \text{ k}\Omega\cdot\text{cm}^{-2}$  due catalytic effect or conductivity of the CoOcPhOPc layer. For the Au-PA-FeOcPhOPc the  $R_{CT}$  was  $0.69 \text{ k}\Omega\cdot\text{cm}^{-2}$  and  $1.10 \text{ k}\Omega\cdot\text{cm}^{-2}$  for Au-PA-Mn(OAc)OcPhOPc. The increase in the RCT was

observed for Au-PA-FeOcPhOPc and Au-PA-Mn(OAc)OcPhOPc and this was attributed to the The fitted circuit elements were summarized in Table 1.

Table 2 The CV and EIS results of the characterization of the bare Au, Au-PA and Au-PA-MOcPhPc (M = Fe, Co, and Mn) in  $2.0 \text{ mmol}\cdot\text{L}^{-1} \text{ K}_3/\text{K}_4[\text{Fe}(\text{CN})_6]$  containing  $0.10 \text{ mol}\cdot\text{L}^{-1} \text{ KCl}$ .

Electrode	Cyclic voltammetry		Nyquist plot		CPE ( $\mu\text{F}$ )	n	$Z_w$ ( $\mu\Omega$ )
	$\Delta E$ (mV)	$E_{1/2}$ (mV)	$R_s$ (k $\Omega$ )	$R_{CT}$ (k $\Omega$ )			
Au	$73 \pm 4.40$	205	0.26	0.67	$3.75 \pm 0.28$	0.84	99.50
Au-PA	-	-	0.24	139	$1.61 \pm 0.11$	0.93	64.90
Au-PA-FeOcPhOPc	$127 \pm 2.52$	199	0.07	27.7	$1.91 \pm 0.70$	0.77	61.90
Au-PA-CoOcPhOPc	$154 \pm 4.53$	195	0.28	9.01	$0.78 \pm 0.14$	0.89	67.50
Au-PA-MnOcPhOPc	$188 \pm 2.56$	244	0.06	25.1	$1.89 \pm 0.10$	0.78	56.90

The real surface area of the gold electrode represents the actual are of gold surface after mechanical treatment by polishing in aqueous alumina slurries of 1.0, 0.30 and 0.065 micron. The geometric area calculated using the active surface diameter is  $0.0201 \text{ cm}^2$  and represent an underestimation of the actual electrode surface. Using the electrochemical measurement were can calculate the actual surface area and was found to be  $0.0413 \text{ cm}^2$  using Equation 4.1

$$I_{pa} = (2.69 \times 10^5) n^{3/2} AD^{1/2} Cv^{1/2} \quad (4.1)$$

where 'n' is the number of electrons involved ( $n = 1$ ); A is the geometric surface area of gold electrode ( $A = \text{actual surface area calculated}$ ); C is the concentration of the  $\text{K}_3\text{Fe}(\text{CN})_6$  is ( $2.0 \text{ mmol}\cdot\text{L}^{-1}$ ), D is the diffusion coefficient of  $\text{K}_3\text{Fe}(\text{CN})_6$  is  $7.6 \times 10^{-6} \text{ cm}^2\cdot\text{s}^{-1}$  and v is the scan rate ( $0.050 \text{ V}\cdot\text{s}^{-1}$ ). The surface roughness, is the ratio of the real surface area ( $0.0413 \text{ cm}^2$ ) and the geometric area ( $0.0201 \text{ cm}^2$ ) is 2.05. The real surface area was used in all other surface area calculations.

#### • Under Potential Deposition of Copper (Cu-UDP) and Gold Oxidation

Figure 18 shows the cyclic voltammograms of the (i) bare Au, (ii) Au-PA, and (iii) Au-PA-CoOcPhOPc in (a) in  $2.0 \text{ mmol}\cdot\text{L}^{-1} \text{ CuSO}_4$  containing  $0.50 \text{ mol}\cdot\text{L}^{-1} \text{ H}_2\text{SO}_4$  and (b)  $0.01 \text{ mol}\cdot\text{L}^{-1} \text{ KOH}$  solution. In Figure 18 (a)(i), the bare gold electrode displayed two reduction peaks (I) due to metal reduction from  $\text{Cu}^{\text{II}}$  to  $\text{Cu}^{\text{I}}$  at  $0.225 \text{ V}$ . The second reduction peak (II) was observed at  $-0.015 \text{ V}$  due to the metal reduction of  $\text{Cu}^{\text{I}}/\text{Cu}^0$ . The metallic  $\text{Cu}^0$  deposits onto the gold electrode surface, thereby forming Cu ad-atom formation. The return scan displayed a notable large anodic peak at  $0.020 \text{ V}$  due to the stripping of metallic ( $\text{Cu}^0$ ) copper layer from the gold surface and oxidation  $\text{Cu}^0$  to form  $\text{Cu}^{\text{I}}$  and dissolving back into solution. Upon scanning further in the oxidation potential,  $\text{Cu}^{\text{I}}$  to  $\text{Cu}^{\text{II}}$  peak was observed at  $0.242 \text{ V}$ . In Figure 18 (a)(ii) for Au-PA, the copper reduction-oxidation peaks at similar potential values was observed with decreased currents. The decrease in peak

currents was due to PA thin layer that was electrografted onto the gold electrode surface. The deposited copper was at pinholes. In Figure 18 (a)(iii), Au-PA-CoOcPhOPc, the reduction and stripping of  $\text{CuSO}_4$  solution was blocked and very small redox peak due to copper were observed. The further decrease was due to the deposited CoOcPhOPc thin monolayer film after amide coupling reaction. The results confirmed the presence of PA (Au-PA) and PA-CoOcPhOPc onto gold electrode surface, establishing the presence of material (thin film layer of the complex) on the electrode surface.

The complete suppression of the Cu reduction and oxidation reaction was also observed at Au-PA-FeOcPhOPc and Au-PA-Mn(OAc)OcPhOPc surfaces.

The oxidation and reduction reaction of the bare and modified electrodes were studied in  $0.010 \text{ mol}\cdot\text{L}^{-1} \text{ KOH}$  solution. The cyclic voltammograms of the bare Au in Figure 18 (b)(i) shows the gold oxidation peak at  $0.57 \text{ V}$  and the reduction peak  $0.18 \text{ V}$ . The bare gold electrode surface in KOH forms a monolayer of oxygen in the form of gold (I) hydroxide on the forward scan. On the reverse scan, the gold oxide layer is stripped off from the surface of the gold resulting in the broad reduction peak at  $0.18 \text{ V}$ . After the modification of the surface with phenylamino (Au-PA) and with PA-CoOcPhOPc thin films, the CVs in Figure 18 (b)(ii) and (iii) shows that the oxidation and reduction peak currents decreased. The small peak currents were due to solution permeability and reaction at the pin-holes. Both the Au-PA and Au-PACoOcPhOPc showed reactions at pin-holes. The decrease in currents was due to the thin films blocking to some extent the solution ions from reaching the underlying gold surface for oxidation and reduction reactions to occur. The decrease in currents confirmed the formation of PA and PA-CoOcPhOPc thin films. Similar behaviour to Au-PA-CoOcPhOPc was observed for the Au-PA-FeOcPhOPc and Au-PA-Mn(OAc)OcPhOPc surfaces confirming the surface modification.

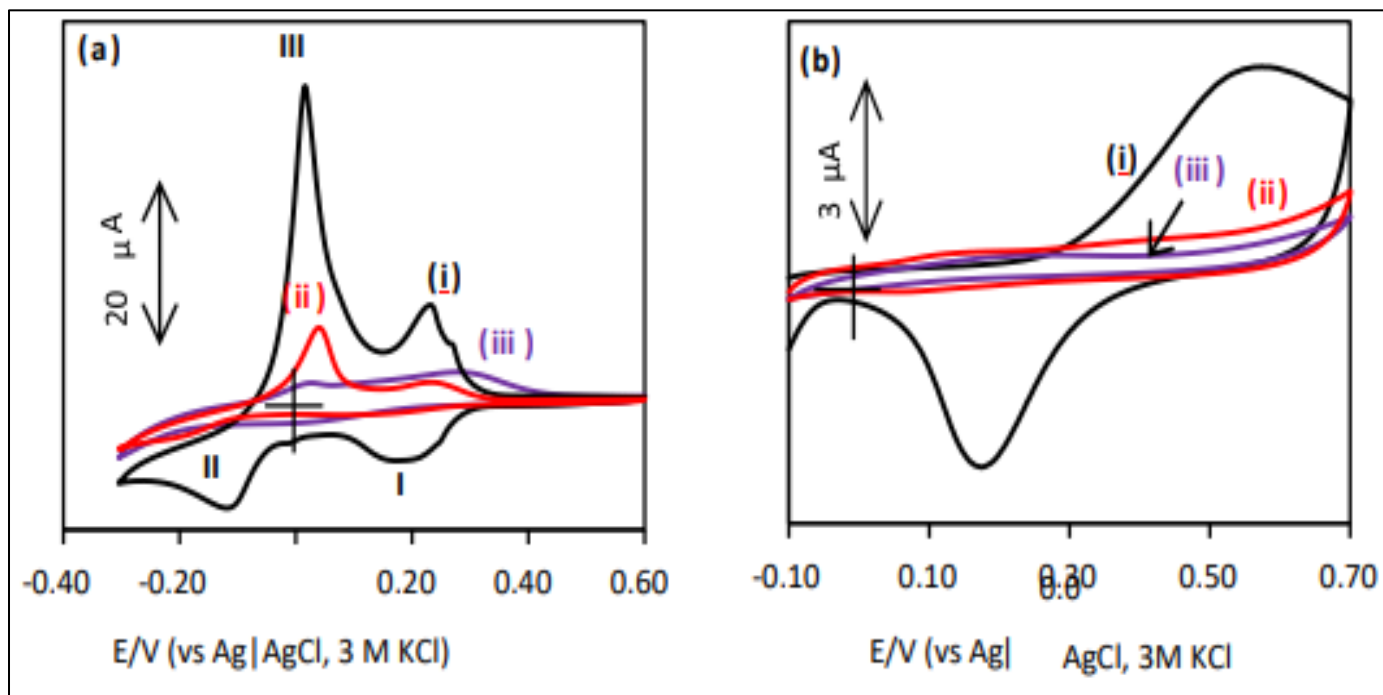


Fig 18 Cyclic voltammograms of (i) Au, (ii) Au-PA, (iii) Au-PA-CoOcPhOPc in (a) 2.0 mM CuSO<sub>4</sub> in 0.50 mol.L<sup>-1</sup> H<sub>2</sub>SO<sub>4</sub> and (b) 0.010 mol.L<sup>-1</sup> KOH solution. Scan rate 100 mVs<sup>-1</sup>.

The ion barrier factor ( $\Gamma_{ibf}$ ), the measure of electrode modification and its interaction with solution ions was measured and calculated using Equation 4.2.

$$\Gamma_{MPC} = \frac{Q_{PA} - MOCPhOPc}{Q_{bare\ Au}} \quad (4.2)$$

The total charge (Q) of the bare and the modified surfaces were obtained by integrating the currents under the peak.  $Q_{bare\ Au}$  for the bare was integrated and obtained to be  $6.38 \times 10^{-7}$  C and the  $Q_{PA-MOCPhOPc}$  or  $Q_{PA}$  for the modified was for the PA and MOCPhOPc modified electrode. For Au-PA-CoOcPhOPc the  $Q_{PA-CoOcPhOPc}$  was obtained to be  $1.53 \times 10^{-7}$  C. The  $\Gamma_{ibf}$  was calculated to be 0.76 for Au-PA-CoOcPhOPc and Au-PA-FeOcPhOPc, and 0.77 for AuPA-Mn(OAc)OcPhOPc. The surface coverage of the complexes on the gold electrode was also calculated using Equation 4.3

$$\Gamma_{MPC} = \frac{QMOCPhOPc}{nFA} \quad (4.3)$$

Where Q is the charge under the reduction peak (Coulombs), F is the Faraday constants ( $96485\text{ C}\cdot\text{mol}^{-1}$ ), n is the number of electrons transferred (1.0) during the redox reaction, A is the geometric area of the gold electrode ( $0.0201\text{ cm}^2$ ). The surface coverage was estimated to be  $7.93 \times 10^{-11}\text{ mol}\cdot\text{cm}^{-2}$  for Au-PA-FeOcPhOPc,  $7.98 \times 10^{-11}\text{ mol}\cdot\text{cm}^{-2}$  for Au-PA-CoOcPhOPc and  $7.69 \times 10^{-11}\text{ mol}\cdot\text{cm}^{-2}$  for Au-PA-Mn(OAc)OcPhOPc. The values obtained are lower than those of phthalocyanines lying flat on the electrode surface or forming an umbrella orientation know to be  $1.0 \times 10^{-10}\text{ mol}\cdot\text{cm}^{-2}$ . The values cover a small surface area and therefore suggesting the perpendicular or vertical

orientation of the MPC complexes on the gold electrode surface as previously reported [19].

• Buffer (Ph 7.4) Studies

Figure 19 shows the CVs of the (i) bare Au, (ii) Au-PA, and (iii) Au-PA-CoOcPhOPc. The CV for the bare Au showed no peak at the studied potential scan range. The Au-PACoOcPhOPc surface showed a metal ion redox process ( $\text{Co}^{\text{III}}\text{Pc}^{-2}/\text{Co}^{\text{II}}\text{Pc}^{-2}$ ) with an oxidation peak at 250 mV and reduction peak at 120 mV. The formal potential ( $E_{1/2}$ ) was found to be 185 mV. Metal redox processes were observed for Au-PA-FeOcPhOPc as  $\text{Fe}^{\text{II}}\text{Pc}/\text{Fe}^{\text{III}}\text{Pc}^{-2}$  and AuPA-Mn(OAc)OcPhOPc as  $\text{Mn}^{\text{III}}\text{Pc}^{-2}/\text{Mn}^{\text{IV}}\text{Pc}^{-2}$ . The oxidation and reduction peaks observed for Au-PA-Mn(OAc)OcPhOPc were 239 mV and 127 mV with  $E_{1/2} = 183\text{ mV}$ . The redox peaks observed on the modified surfaces confirmed the presence of the thin layer film on the electrode surface and was not observed at Au-PA surface.

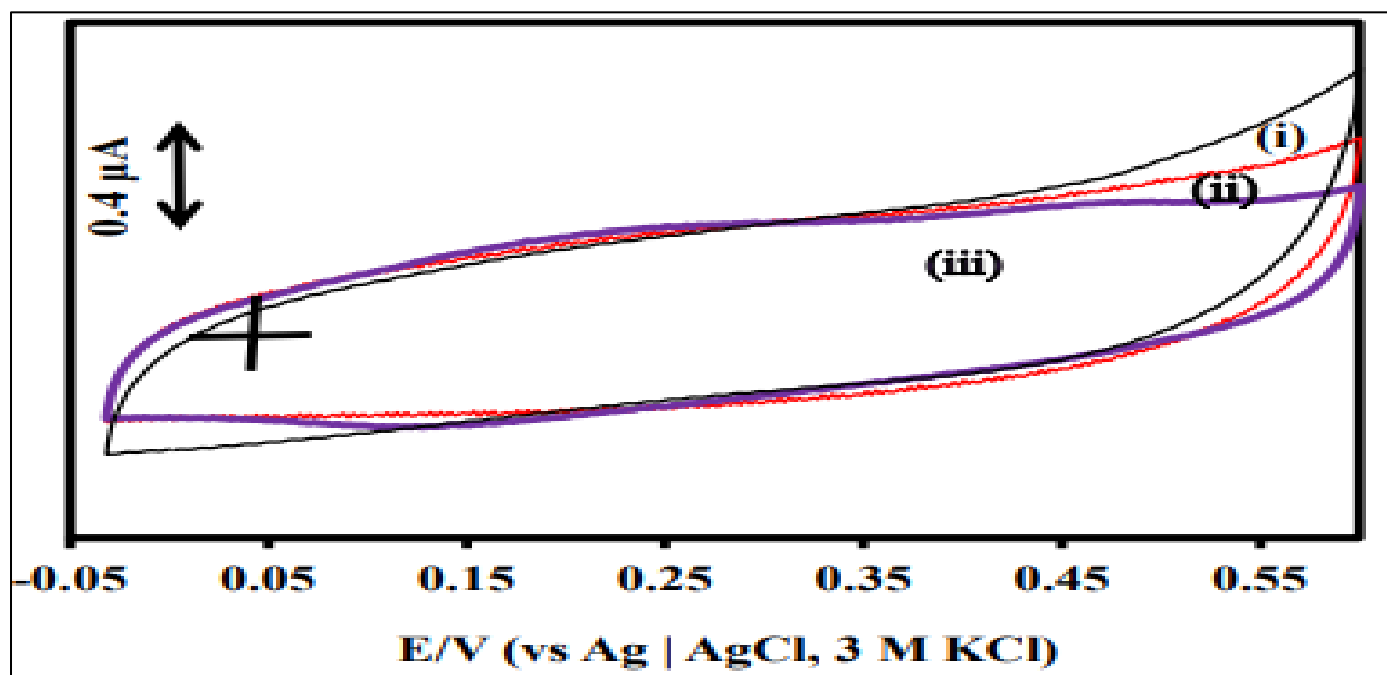
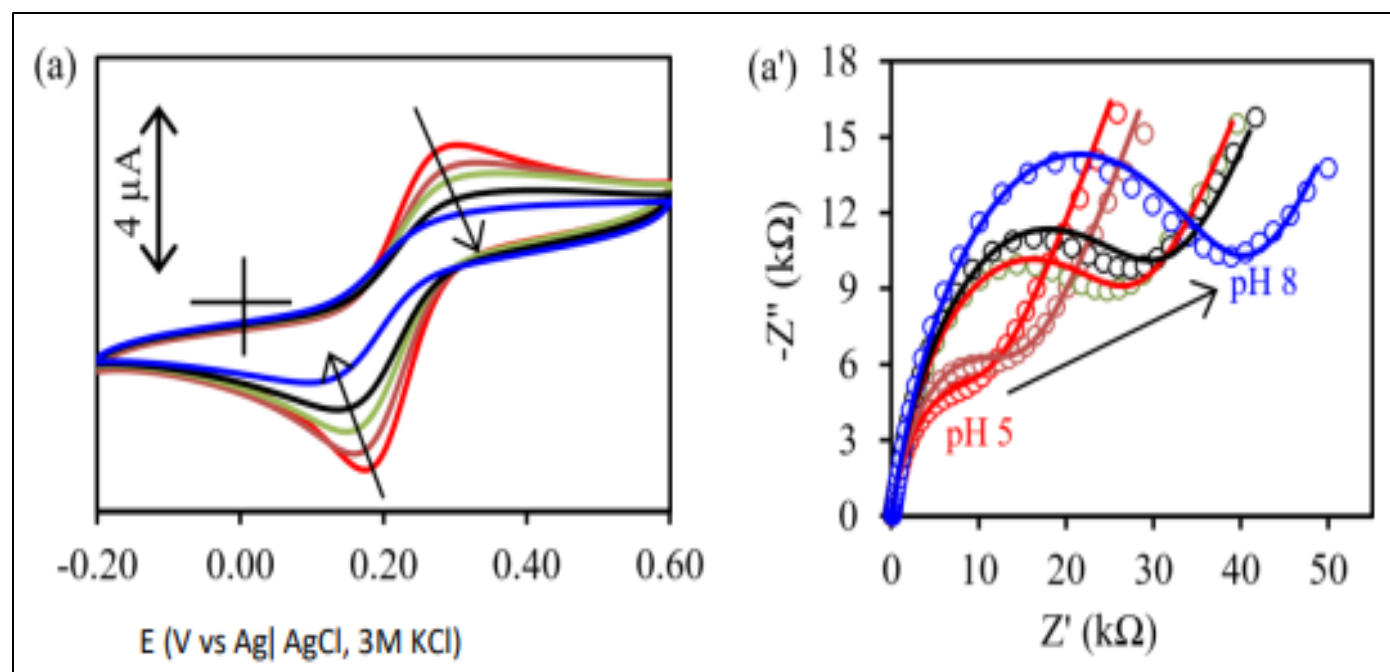


Fig 19 Cyclic voltammograms of (i) bare Au, (ii) Au-PA, and (iii) Au-PA-CoOcPhOPc in 0.10 M phosphate buffer saline (PBS) solution, pH 7.4. The scan rate of 100 mV/s.

• *Effect of pH Studies of Au-PA-MOcPhOPc Towards [Fe(CN)<sub>6</sub>]<sup>3-/4-</sup> Redox Couple*

Figure 20 shows the effect of pH changes for (a) Au-PA-FeOcPhOPc, (b) Au-PACoOcPhOPc and (c) Au-PA-Mn(OAc)OcPhOPc surfaces in 2.0 mmol.L<sup>-1</sup> K<sub>3</sub>/K<sub>4</sub>[Fe(CN)<sub>6</sub>] containing 0.10 mol.L<sup>-1</sup> KCl at different pH solutions ranging from (5.0 to 8.0). For all the complex modified electrodes, the CVs showed a decrease in current and an increase in peak-to-peak separation ( $\Delta E$ ) as the pH increased from 5.0 to 8.0. The decrease was attributed to the deprotonation of carboxylic acid functional group (COO<sup>-</sup>) repelling the negatively charged redox probe, [Fe(CN)<sub>6</sub>]<sup>3-/4-</sup>. The pKa of the carboxylic acid on the peripheral position of

the phthalocyanine complexes is 4.59. Therefore, at pH > 4.59 the COOH is negatively charged (COO<sup>-</sup>). Figure 20 (a' – c') shows Impedance data represented as Nyquist plots for (a) Au-PA-FeOcPhOPc, (b) Au-PA-CoOcPhOPc and (c) Au-PA-Mn(OAc)OcPhOPc surfaces in 2.0 mmol.L<sup>-1</sup> K<sub>3</sub>/K<sub>4</sub>[Fe(CN)<sub>6</sub>] containing 0.10 mol.L<sup>-1</sup> KCl at different pH solutions ranging from (5.0 to 8.0). The Nyquist plots shows the increase in the R<sub>CT</sub> with the increase in pH further confirming pH sensitive and responsive nature of Au-PA-MOcPhOPc surfaces. The pH effect of Au-PA-MOcPhOPc (M = Co, Fe and Mn(OAc)) was further investigated against the positively charged redox probe, [Ru(NH<sub>3</sub>)<sub>6</sub>]<sup>2+/3+</sup>.



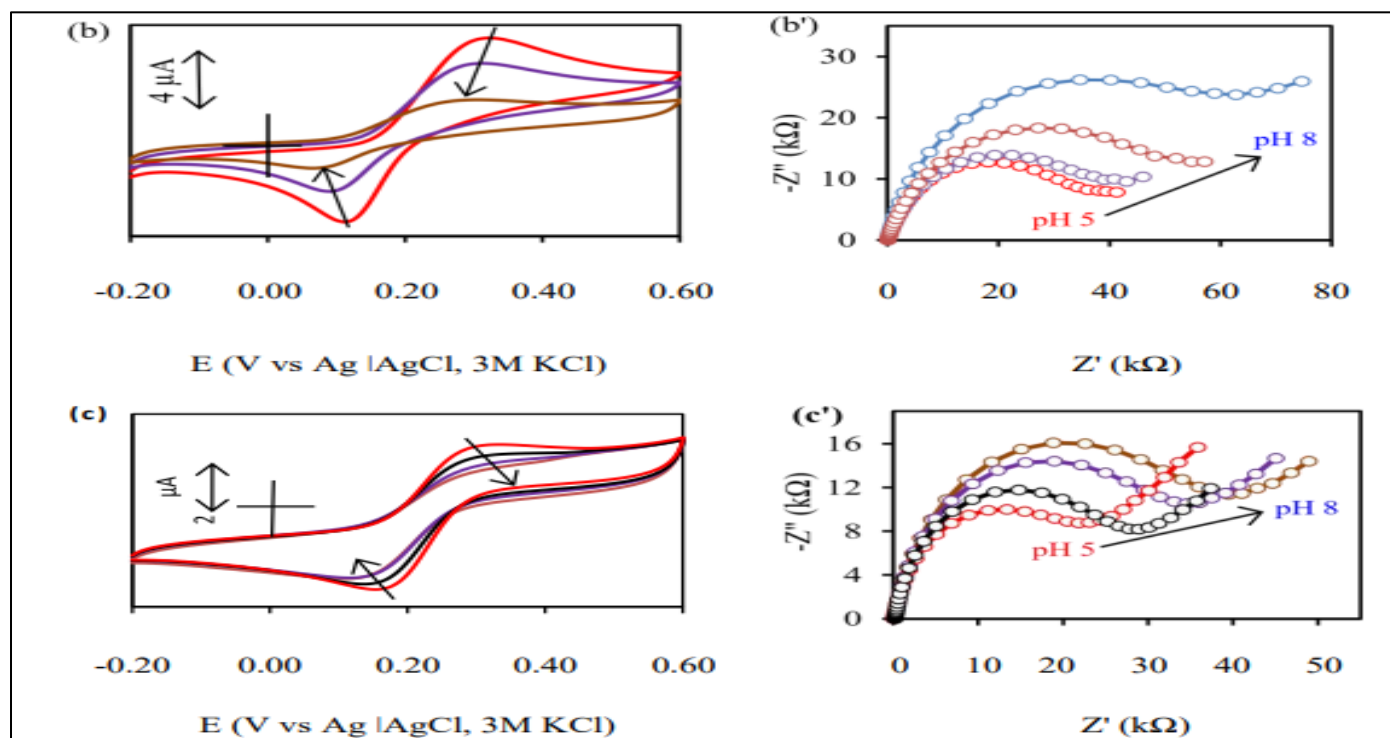


Fig 20 Cyclic voltammograms and impedance spectroscopy (Nyquist plot) for (a) Au-PAFeOcPhOPc, (b) Au-PA-CoOcPhOPc, and (c) Au-PA-Mn(OAc)OcPhOPc in 2.0 mmol.L<sup>-1</sup> K<sub>3</sub>/K<sub>4</sub>[Fe(CN)<sub>6</sub>] containing 0.10 mol.L<sup>-1</sup> KCl at varied pH conditions.

• *Effect of Ph Changes of Au-PA-MOCPhOPc Towards [Ru(NH<sub>3</sub>)<sub>6</sub>]<sup>2+/3+</sup> Redox Probe*

Figure 21 shows the effect of pH changes for Au-PA-CoOcPhOPc, (a) the cyclic voltammograms, and (b) Impedance spectroscopy (Nyquist plots) in 2.0 mmol.L<sup>-1</sup> Ru(NH<sub>3</sub>)<sub>6</sub> containing 0.10 mol.L<sup>-1</sup> KCl at different pH ranging from (3.0 to 8.0). There were no changes in the cyclic voltammograms and impedance spectroscopy (Nyquist plot representation) for all the electrodes. The lack of changes is due to the fact that the pK<sub>a</sub> values for carboxylic acid of the metallophthalocyanines are 4.57. This means that at pH < pK<sub>a</sub>, the carboxylic acid functional groups are neutral (COOH). At pH values > pK<sub>a</sub>, the carboxylic acid functional groups are deprotonated (COO<sup>-</sup>).

There is therefore attractive forces between the COO<sup>-</sup> and [Ru(NH<sub>3</sub>)<sub>6</sub>]<sup>2+/3+</sup> and hence the observed redox couple due at Au-PA-CoOcPhOPc. The COOH functional groups behave the same for the MOCPhOPc modified electrodes (Au-PAMOCPhOPc, M = Co, Fe and Mn). The impedance spectroscopy (Nyquist plot representation) showed a Warburg Impedance (Z<sub>w</sub>) with semi-infinite straight line. The observation confirms the oxidation and reduction of Ru(NH<sub>3</sub>)<sub>6</sub> at electrodes even after modifying with octacarboxyphenoxy phthalocyanine complexes. This is preliminary to the electrocatalysis and shows the pH sensitive effect of the modified gold electrodes with complexes bearing carboxylic acid functional groups.

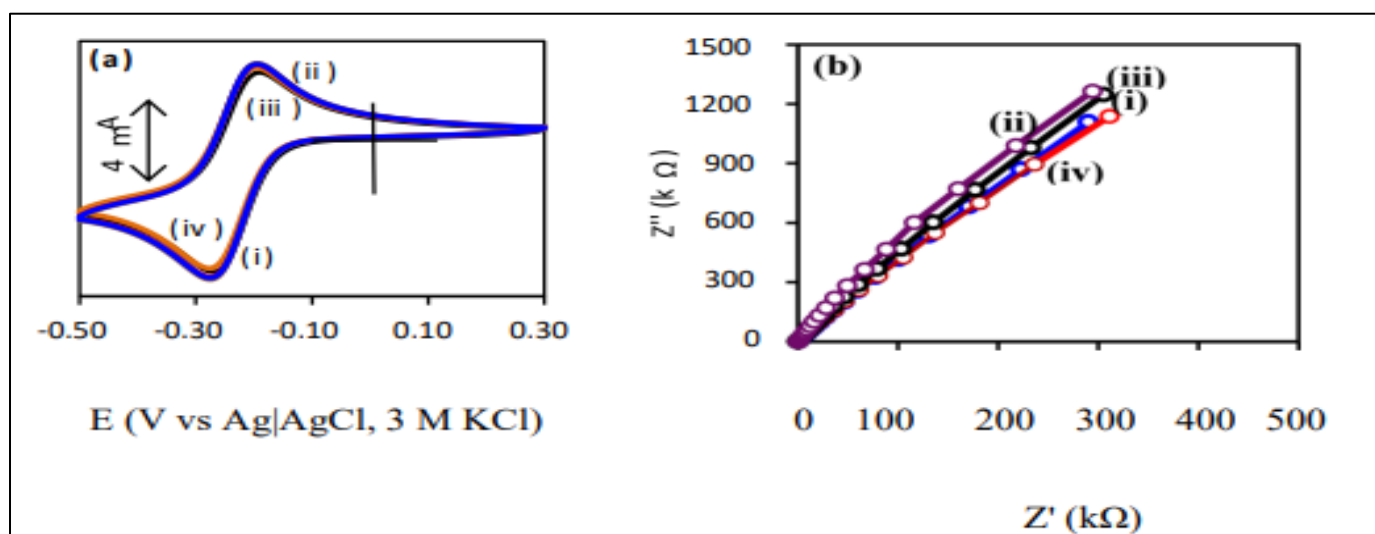


Fig 21 (a) Cyclic voltammograms (CVs) and (b) Impedance spectroscopy (Nyquist plots) of the effect of pH on 2.0 mM [Ru(NH<sub>3</sub>)<sub>6</sub>]<sup>2+/3+</sup> containing 0.10 M KCl at Au-PA-CoOcPhOPc.

#### IV. ACKNOWLEDGEMENT

Akinyemi, Abosede. wishes to acknowledge with thanks Chemistry department, both at Rhodes University, South Africa and Lagos State university of Education, Ijanikin, Lagos State, for the provision of research facilities for this work and for the fund given. Dr Akinyemi Abosede mostly thank my supervisor, Prof. Mashazi, P.N. for his assistance, support and opportunity given to work with him.

- Funding Declaration: The programme was sponsored by Nigeria, TERTfund. Much appreciated.

#### V. CONCLUSION

The 2, 3, 9, 10, 16, 17, 23, 24-octacarboxyphenoxy metallophthalocyanines with different central metals (Fe, Mn, and Co) were synthesized and covalently immobilised onto gold electrodes. The electrodes were pre-modified through electrochemical grafting of 4-nitrobenzene tetrafluoroborate diazonium salt to form phenylnitro radical surface (Au-PNO<sub>2</sub>). The Au-PNO<sub>2</sub> was electrochemically reduced in methanol:water (1:10 by v:v) to form phenylamine gold electrode surface (Au-PA). The metallophthalocyanines complex was immobilized on the Au-PA via amide coupling forming Au-PA-MOCPhOPc.

#### REFERENCES

- [1]. M. D. Brown, M. H. Schoenfish, Catalytic selectivity of metallophthalocyanines for electrochemical nitric oxide sensing, *Electrochim Acta*, 2018 (273) 98–104.
- [2]. M. Grobosch, C. Schmidt, R. Kraus, M. Knupfer, Electronic properties of transition metal phthalocyanines: The impart of the central metal atom ( $d^5-d^{10}$ ), *Organic Electronics* 2010, 11, (9) 1483–1488.
- [3]. T. Koczorowski, W. Szczolko and T. Goslinski, Physicochemical properties and catalytic applications of iron porphyrines and phthalocyanines, *Recent progress in organometallic chemistry*, 2017 (5) 101-121.
- [4]. C. G. Claessens, U. Hahn, T. Torres, Phthalocyanines: From outstanding electronic properties to emerging applications, *The Chemical Record*, 2008 (8) 75–97.
- [5]. S. H. Kim, J. W. Namgoong, S. B. Yuk, J. Y. Kim, W. Lee, C. Yoon, J. P. Kim, Synthesis and characteristics of metal-phthalocyanines tetrasubstituted at non-peripheral (a) or peripheral (b) positions, and their applications in LCD color filters, *Journal of Inclusion Phenomena Macroscopic Chemistry* 2015 (82) 195–202.
- [6]. R. Li, X. Zhang, P. Zhu, D. K. P. Ng, N. Kobayashi, and J. Jiang, Electron-donating or withdrawing nature of substituents revealed by the electrochemistry of metal-free phthalocyanines, *Inorganic Chemistry*, 2006 (45) 2327–2334.
- [7]. M. G. Waltera, A. B. Rudineb and C. C. Wamser, Porphyrins and phthalocyanines in solar photovoltaic cells, *Journal of Porphyrins and Phthalocyanines*, 2010 (14) 759–792.
- [8]. R. Burkitt, T. R. Whiffen, E. H. Yu, Iron phthalocyanines and MnOx composite catalysts for microbial fuel cell applications, *Applied Catalysis B: Environmental* 2016 (181) 279-288.
- [9]. D. D. Eley, Phthalocyanines as semiconductors, *Nature* 1948 (4125) 819.
- [10]. P. Vasudevan, N. Phougat and A. K. Shukla, Metal phthalocyanines as electrocatalysts for redox reactions, review, *Applied Organometallic Chemistry*, 1996, 10 (8) 591-604.
- [11]. T. Ndlovu, O. A. Arotiba, S. Sampath, R. W. Krause and B. B. Mamba, An exfoliated graphite-based bisphenol an electrochemical sensor, *Sensors* 2012 (12) 11601-11611.
- [12]. B. O. Agboola and K. I. Ozoemena, Self-assembly and heterogeneous electron transfer properties of metallo-octacarboxyphthalocyanine complexes on gold electrode, *Physical Chemistry Chemical Physics*, 2008 (10) 2399–2408.
- [13]. S. Boland, F. Barrière and D. Leech, Designing stable redox-active surfaces: chemical attachment of an osmium complex to glassy carbon electrodes prefunctionalized by electrochemical reduction of an in-situ-generated aryldiazonium, *Langmuir* 2008, 24 (12) 6351-6358.
- [14]. L. Cheng, X. Ge and L. Huang, Direct amidation of non-activated phenyl acetic acid and benzylamine derivatives catalysed by NiCl<sub>2</sub>, *Royal Society Open Science*, 2018 (5) 171870.
- [15]. J. R. Dunetz, J. Magano and G. A. Weisenburger, Large-scale applications of amide coupling reagents for the synthesis of pharmaceuticals, *Organic Process Research Development*, 2016 20 (2) 140-177.
- [16]. S. E. Maree and T. Nyokong, Syntheses and photochemical properties of octasubstituted phthalocyaninato zinc complexes, *Journal of Porphyrins Phthalocyanines* 2001 (5) 782–792.
- [17]. P. J. Stephens, Theory of magnetic circular dichroism. *The Journal of Chemical Physics*, 1970 52 (7) 3489.
- [18]. P. N. Mashazi, P. Westbroek, K. I. Ozoemena, T. Nyokong, Surface chemistry and electrocatalytic behaviour of tetra-carboxy-substituted iron, cobalt and manganese phthalocyanines self-assembled monolayers on gold electrode. *Electrochimica Acta* 2007 (53) 1858-1869.
- [19]. M. A. Rauf, S. Hisaindee, J.P. Graham, M. Nawaz, Solvent effects on the absorption and fluorescence spectra of Cu (ii) phthalocyanines and DFT calculations, *Journal of Molecular Liquids* 2012 (168) 102-109.